

ICRH antenna coupling physics and optimum plasma edge density profile. Application to ITER

This content has been downloaded from IOPscience. Please scroll down to see the full text.

2011 *Plasma Phys. Control. Fusion* 53 085020

(<http://iopscience.iop.org/0741-3335/53/8/085020>)

View the [table of contents for this issue](#), or go to the [journal homepage](#) for more

Download details:

IP Address: 136.206.1.12

This content was downloaded on 23/03/2015 at 12:30

Please note that [terms and conditions apply](#).

ICRH antenna coupling physics and optimum plasma edge density profile. Application to ITER

A Messiaen and R Weynants

Laboratory for Plasma Physics, Association EURATOM–Belgian State, Partner in the Trilateral Euregio cluster, Royal Military Academy, B-1000 Brussels, Belgium

E-mail: a.messiaen@fz-juelich.de

Received 16 February 2011, in final form 17 May 2011

Published 23 June 2011

Online at stacks.iop.org/PPCF/53/085020

Abstract

The performance of an ICRH system depends on the coupling capabilities of the antenna to the inhomogeneous plasma profile in front of it. The aim of this study is to understand the key physics phenomena contributing to the coupling. It is shown that the following plasma density profile characteristics are decisive: (i) distance between the antenna and the wave cutoff density, (ii) position of an optimum density with respect to the cutoff one and (iii) the density gradient leading from this optimum density to the plasma bulk. At each step of the analysis approximate relations are derived and the loading due to the plasma is compared with that of an isotropic dielectric medium in view of the application for modelling or dummy load testing. Examples are taken starting from the case of the projected ITER antenna array with its different phasing cases in front of the plasma edge profile used in the conceptual design phase. It is shown that, for the same antenna–cutoff distance, slight profile modifications can lead to substantial coupling and therefore power capability variations. Stronger profile modifications and some critically shaped resonant edge profiles are also analysed. The usefulness of a dielectric medium to simulate plasma loading is discussed in an appendix.

(Some figures in this article are in colour only in the electronic version)

1. Introduction

A critical issue of ICRF heating or current drive is the coupling of the rf waves through the plasma boundary layer to the bulk plasma where absorption is taking place. The aim of this study is to understand the key physics phenomena contributing to the coupling, derive an optimal profile and find what profile modifications to a given profile could improve the power capability of an ICRH system. It should be said right away that the way to produce such changes and their effect on confinement is not considered here. In preceding coupling studies the determining influence of the antenna–cutoff distance, of the plasma density gradient and

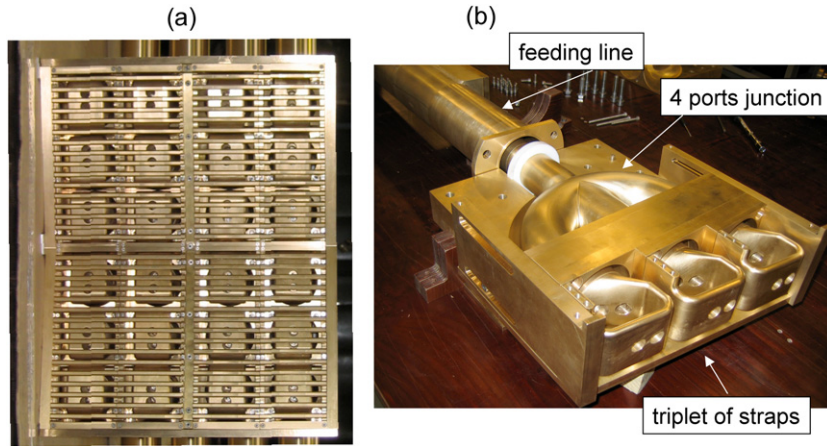


Figure 1. (a) Front view of the 24 straps array (grouped in eight triplets) behind the Faraday screen; (b) view of one single strap triplet fed by its 4-port junction.

of their complex interplay have already been underlined [1–4]. In a recent analysis of the expected performances of the ITER ICRF antenna array the strong influence of the toroidal and poloidal phasings of the array elements has been pointed out [5, 6]. In this paper we will systematically analyse the influence of the characteristics of the edge plasma profile shape on the coupling performances for different antenna phasing conditions. Our reference situation is the ITER antenna array facing the plasma profile that was considered earlier while analysing the performance dependence on phasing [5]. The reference condition is summarized in section 2. Also given there is an introduction to the needed theoretical relations of the modelling made by the ANTITER II code (see the appendix of [5]). At each step of the analysis we will also make a comparative evaluation of the antenna coupling to an isotropic dielectric medium (such as e.g. water) in view of its application for modelling and for dummy load testing. The plasma loading simulation by an isotropic dielectric medium has been summarized in [7] and is further discussed and concluded in the appendix.

2. Reference antenna array and plasma profile. Discussion of their modelling

We consider as reference situation one of the two planned ITER ICRF antennas of the baseline design [8]. It is constituted by an array of 24 short straps grouped in 8 triplets by means of 4-port junctions allowing various heating and current drive phasing with load resilience in the frequency band 40–55 MHz and a nominal radiated power capability of 20 MW per antenna. Figure 1 shows (a) a view of the 24-strap array behind the Faraday screen and (b) one single strap triplet with the antenna boxes cut-away for display and fed in parallel by a 4-port junction. The pictures are taken from the scaled (1/4) mock-up of the present version of the antenna plug electrical design.

The coupling is expressed [5, 9] by the mean conductance of the triplet feeding lines $G_{\min 3} = 2P/|V_{\max}|^2$, P being the mean active radiated power $P_{\text{tot}}/8$ of the 8 triplets (P_{tot} is the total radiated power by the array) and $|V_{\max}|$ the antinode voltage amplitude applied on the 8 feeding lines of the plug. $G_{\min 3}$ depends on the toroidal and the poloidal phasing of the triplets imposed by the phasing of V_{\max} [5, 9]. To obtain the load resilience each poloidal triplet pair is fed by a quadrature hybrid (through matching and decoupling circuits), which

Table 1. Values of $|k_z M|$ and $k_y M$ selected by the considered phasing cases. The corresponding values of N_{CO} and K_{DCO} for $f = 46.5$ MHz are added.

Case	$ k_z M $	$k_y M$	N_{CO}	K_{DCO}
1 $0\pi 0\pi$	7.5 m^{-1}	1.25 m^{-1}	$4.4 \times 10^{18} \text{ m}^{-3}$	61
2 $00\pi\pi$	3.1	0.9	0.71	11
3 $0\pi\pi 0$	4.6	1.3	1.6	24
4 $0\pi/2\pi 3\pi/2$	3.65	1.9	1.1	16
5 $0-\pi/2-\pi -3\pi/2$	3.85	0.45	1.1	16

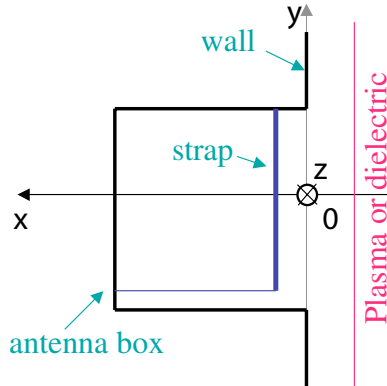


Figure 2. Section of one recessed antenna box excited by a thin strap.

imposes a poloidal phasing of $\pm\pi/2$. The four hybrids are delivering the same power $P_{\text{tot}}/8$ to the 8 triplets if appropriate decouplers are used to cancel the effect of mutual coupling between the triplets [8]. We consider the five cases of toroidal phasing given in table 1 with equal current amplitude in the eight triplets (as proposed for the decoupling-matching system described in [9]).

The antenna is modelled by the fast code ANTITER II [5], which was satisfactorily benchmarked to the Topica code [5]. It is described as an array of antenna boxes recessed in the wall (position $x = 0$), each box being excited by a thin radiating strap (see figure 2). A vacuum layer of thickness a ($\equiv |x_{\text{edge}} - x_{\text{antenna}}|$) is assumed in front of the boxes followed by the inhomogeneous plasma layer (from $x = -x_{\text{edge}}$ to $x = -x_{\text{bulk}}$) and by a semi-infinite homogeneous bulk plasma where complete (i.e. single pass) absorption is assumed. As reference plasma profile we choose in this paper the profile shown in figure 3 having an exponential decay with a constant decay length of 2.4 cm starting from a bulk electron density $N = 10^{20} \text{ m}^{-3}$ at a distance $x_{\text{bulk}} = 23$ cm from the antenna. Note that this profile has been shown [5] to be an excellent approximation to the not too optimistic ‘Sc2 short 17’ profile provided by ITER IO [10] (based on modelling described in [11]) for the antenna conceptual design.

ANTITER II describes the radiated waves in plane geometry by a Fourier analysis in $\exp(-i\omega t + ik_z z + ik_y y)$ with $\omega = 2\pi f$, where f is the frequency and k_z is the propagation constant along the steady magnetic field and k_y the one perpendicular to the latter and to the radial outward x direction. The tangential field components at the box apertures are matched to the Fourier integral expansion in the outside medium. We assume that only the TE $/z$ (transverse electric with respect to the z -axis) field component is excited through a perfect Faraday screen placed at the box apertures. Inside the plasma we consider the coupling to the

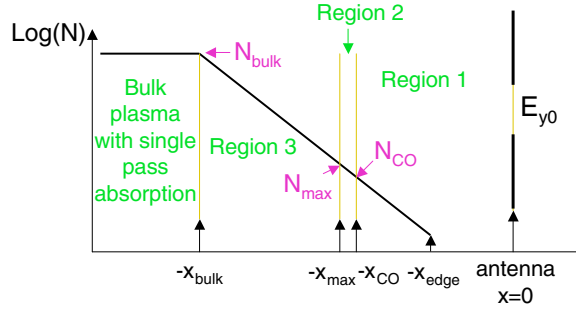


Figure 3. Considered inhomogeneous density (or dielectric constant) profile in front of the antenna array with the regions controlling the coupling to the bulk plasma (or dielectric), where complete absorption is assumed.

fast Alfvén waves. They are described by the set of differential equations

$$\frac{d/dx}{E_y} \begin{vmatrix} i\omega B_z \\ E_y \end{vmatrix} = \begin{vmatrix} -\mu k_y & -k_\perp^2 \\ 1 - k_y^2/u & \mu k_y \end{vmatrix} \begin{vmatrix} i\omega B_z \\ E_y \end{vmatrix}, \quad (1)$$

where $k_\perp^2 = k_0^2 \varepsilon_1 - k_z^2 - \mu k_0^2 \varepsilon_2$, $\mu = k_0^2 \varepsilon_2 / (k_0^2 \varepsilon_1 - k_z^2)$, $u = k_0^2 \varepsilon_1 - k_z^2$ and $k_0 = \omega/c$ (c : vacuum light velocity). ε_1 and $i\varepsilon_2$ are the xx ($=yy$) and xy cold plasma dielectric tensor terms. In the ICRF domain, for single species cold plasma we have $\varepsilon_1 = 1 - \omega_{pi}^2 / (\omega^2 - \omega_{ci}^2)$ and $\varepsilon_2 = -\omega_{pi}^2 / (\omega^2 - \omega_{ci}^2)$ (ω/ω_{ci}). ω_{pi} and ω_{ci} are, respectively, the ion plasma and cyclotron frequencies. For dielectric the same equations can be used with $\varepsilon_1 = K_D = K'_D + iK''_D$ (K_D being the complex dielectric constant) and $\varepsilon_2 = 0$.

The ratio $\xi(k_z, k_y, x) = E_y / (\omega B_z)$ defines the normalized surface impedance in x ; $1/\xi$ is the normalized surface admittance. As boundary condition at $x = x_{bulk}$, where no reflection is assumed from the homogeneous bulk plasma of electron density N_{bulk} , we have, for waves propagating towards $x < 0$, $\xi_{p,bulk}(k_z, k_y) = (E_y / (\omega B_z))_{x=x_{bulk}} = \{-i(\mu k_y - i\rho)/k_\perp^2\}_{x=x_{bulk}}$ with the x -direction propagation constant in the uniform bulk plasma given by $\rho = (k_\perp^2 - k_y^2)^{1/2}$. Each wave from the Fourier expansion is non-propagating if $k_\perp^2 - k_y^2 < 0$. This corresponds in vacuum to $k_0^2 - k_z^2 - k_y^2 < 0$ and for plasma to an electron density below the cutoff one N_{CO} . N_{CO} is given for $k_y = 0$ by the solution of $k_z^2/k_0^2 = \varepsilon_1(x) - \varepsilon_2(x)$ that is given by $N_{CO} \propto (\omega_{pi}^2)_{CO} = (k_z^2 - k_0^2)(\omega_{ci}^2 + \omega\omega_{ci})/k_0^2$ for single species plasma. For dielectric the radial propagation constant is given by $\rho_d = (k_{\perp d}^2 - k_y^2)^{1/2} = (k_0^2 K_D - k_z^2 - k_y^2)^{1/2}$ and the cutoff dielectric constant by $K'_{D,CO} = (k_z^2 + k_y^2)/k_0^2$ (for $K''_D = 0$).

The total radiated power is obtained from the Poynting theorem applied at the box aperture ($x = 0$):

$$\begin{aligned} 2P_{tot} &= Re \left\{ (1/(2\pi)^2) \iint E_y H_z^* dk_z dk_y \right\} \\ &= \{1/(4\pi^2 \omega \mu_0)\} Re \left\{ \iint |E_y|^2 / \xi_0^* dk_z dk_y \right\}, \end{aligned} \quad (2)$$

where $|E_y(k_z, k_y)|^2$ is the excitation function of the array on the aperture and $1/\xi_0(k_z, k_y) = \omega B_z / E_y$ is the normalized surface admittance of the external medium (vacuum layer + inhomogeneous plasma) in front of the antenna array. The antenna array phasing selects in the k_z, k_y plane some small regions centred on $k_z = k_{zM}$ and $k_y = k_{yM}$ which have significant contribution to the coupling. Figure 4 shows a 3D view of the k_y, k_z spectrum

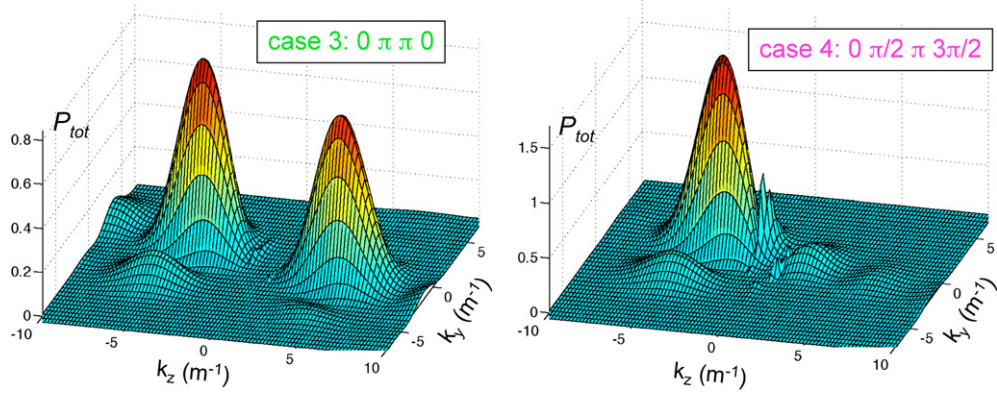


Figure 4. 3D view of the radiated power spectrum $P_{\text{rad}}(k_z, k_y)$ for the phasing cases 3 and 4.

of P_{tot} for a heating and a current drive case. The heating phasing selects mainly two regions, approximately symmetric in $\pm|k_z|$ and of mean maximum $\langle k_{yM} \rangle$ value, the asymmetry being due to the poloidal steady magnetic field, whereas the current drive one selects mainly one single region. The values of $|k_{zM}|$ and k_{yM} for the five considered toroidal phasing cases are given in table 1 together with the corresponding $N_{\text{CO}}(|k_{zM}|, \langle k_{yM} \rangle)$ and $K_{\text{DCO}}(|k_{zM}|, \langle k_{yM} \rangle)$ (for $K_D'' = 0$). ANTITER II computes the coupling for the entire wave spectrum but the study of the Fourier wave component for $k_z = k_{zM}$ and $k_y = k_{yM}$ describes to a good approximation the wave behaviour resulting from the whole spectrum. An approximate expression for the active radiated power is given by

$$P_{\text{tot}} \propto \text{Re}\{1/\xi_0^*(|k_{zM}|, k_{yM})\} \iint_{\mathfrak{N}} |E_{y0}|^2 dk_z dk_y, \quad (3)$$

where ξ_0 is the surface impedance in front of the antenna ($x = 0$), E_{y0} the Fourier transform of the applied E_y field at the antenna output and where \mathfrak{N} is a k_z, k_y region around $|k_{zM}|, k_{yM}$ with significant contribution to the coupling. The amplitude of E_{y0} is a slowly varying function of k_z, k_y , and is weakly sensitive to the phasing and to the plasma profile.

Typical results from ANTITER II are illustrated in figure 5. In this paper we assume a D plasma with $\omega = 2\omega_{cD}$. Note that the shape of the edge dispersion relation for a DT plasma (50% D, 50% T) with $f = 53$ MHz and $B_0 = 3.9$ T is similar [7]. Figure 5(a) shows for the considered toroidal phasing cases the evolution of $G_{\min 3}$ versus frequency in and around the ITER frequency band. A nearly flat response in the ITER band is obtained by inserting a stub (also used as service stub for cooling) in parallel in each triplet feeding line [5, 12]. The effect of the poloidal steady magnetic field is taken into account by tilting the antenna array with respect to the total steady magnetic field B_0 [5]. An antenna tilting angle of 15° is taken here for all considered plasma profiles. It leads to different coupling values for the co- and counter-current drive cases [5]. The value of $G_{\min 3}$ corresponding to a total active radiated power P of 20 MW for an antinode voltage $V_{\max} = 45$ kV in the eight feeding lines is also indicated in the figure. Figure 5(b) shows the contours of the corresponding surface conductance spectrum $\text{Re}\{1/\xi_0(k_y, k_z)\}$ at the output of the antenna array entering equations (2) and (3). This spectrum is an even function of k_z but not of k_y as a result of the plasma gyrotropy. One notes a contribution to the coupling from the coaxial modes [13] with dispersion relation $k_z^2 + k_y^2 \cong k_0^2$ appearing on the surface conductance spectrum shown in figure 5(b). These modes are only weakly excited [5] because the region $|k_z| < k_0$ of the power spectrum is almost depleted for the considered heating and current drive phasing

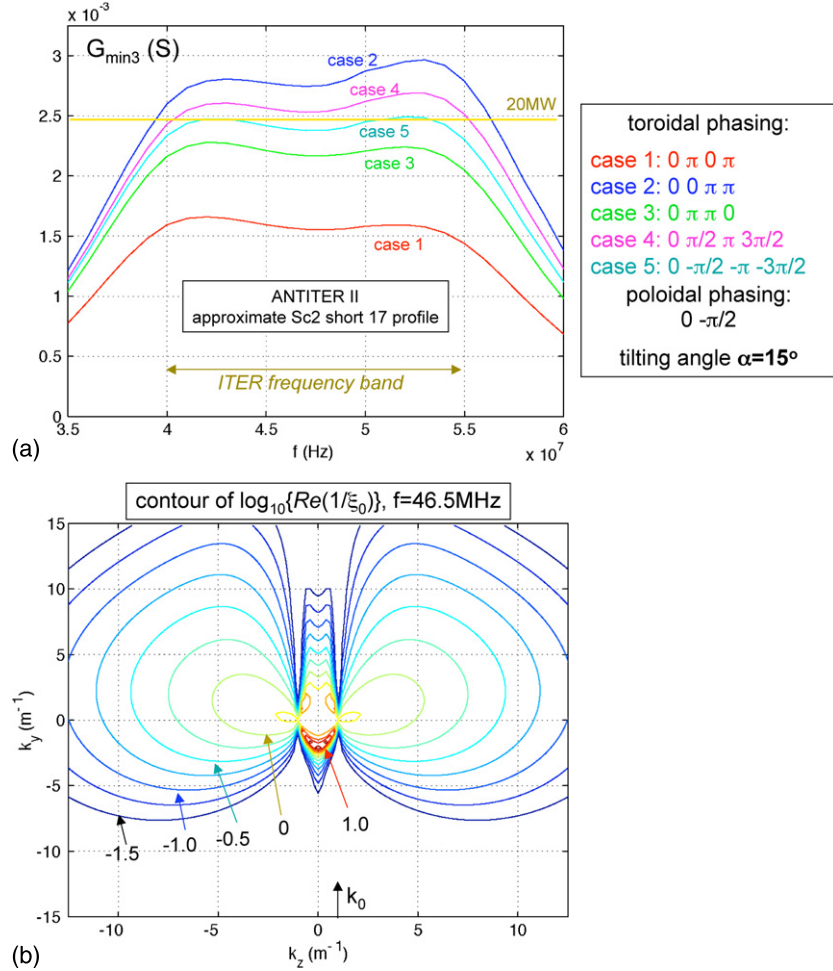


Figure 5. (a) Mean minimum conductance $G_{\min 3}$ in the eight feeding lines as a function of the frequency for the different phasing cases and the reference plasma profile. (b) Contour in the k_z , k_y plane of the surface conductance of the external medium in front of the array ($x = 0$) for the reference plasma profile.

cases of the array (for which the same current amplitude in the eight triplets is assumed). In contrast to the toroidal monopole phasing (0 0 0 0) case, which is only interesting to produce plasma for wall conditioning, coaxial modes are strongly excited. The surface modes [13, 14] characterized by large $k_y > 0$ and have no significant contribution to the coupling for the case of the reference plasma profile. In section 8.2 we discuss a profile leading to possible surface wave contribution to the coupling and in the appendix we show cases of dielectric loading with significant excitation of surface waves.

3. Summary of coupling physics

It is the purpose of this paper to show that the level of ICRF coupling to a decaying plasma profile is set by and depends on the characteristics of the three regions identified in figure 3.

(i) Region 1 from the antenna to the wave cutoff density (N_{CO} , corresponding to the chosen antenna array phasing). The coupling is very sensitive to the width x_{CO} of this region and rather weakly influenced by the presence of density $N < N_{\text{CO}}$. (ii) Region 2 extending from the cutoff density to N_{max} (N_{max} being a few times N_{CO} and defined in section 4). The coupling is sensitive to the width of this region. (iii) Region 3 between N_{max} and N_{bulk} . Here the coupling is very sensitive to the density gradient and its shape.

We now proceed to ascertaining the different impacts of these regions on the coupling properties. (i) First, we study analytically in section 4 the wave coupling to a uniform plasma (or dielectric medium) through a vacuum region. It is shown that the optimum coupling is obtained for a plasma density N_{max} above the cutoff one, set by the antenna phasing and the vacuum zone thickness. The optimum coupling value itself has a strong dependence on the zone thickness. (ii) We then show in section 5 that the presence of density $N < N_{\text{CO}}$ in region 1 does not significantly increase the coupling to the propagating region and that the coupling is maximum when the thickness of region 2 (i.e. distance $N_{\text{CO}} - N_{\text{max}}$) vanishes. (iii) Wave reflection due to a density gradient is the dominant effect in region 3 and is studied in section 6. The existence of minima and maxima of coupling is shown as a function of the density decay length due to multiple reflections. The coupling remains low as long as the decay length is too short to give rise to the first maximum of coupling. (iv) The combined effect of changing the magnitude of the density gradient up to the bulk and the location from where it starts is studied in section 7. (v) Finally in section 8 the effect of deviation in region 3 of the density decay with respect to an exponential one is investigated. It is shown that profiles more hollow than the exponential one can lead to large constructive wave interference resulting in very selective coupling resonances.

It should be noted that our results can also be transposed to the coupling to an inhomogeneous dielectric medium characterized by its dielectric constant profile $K_D(x)$. Figure 3 applies then with N_{bulk} , N_{max} , N_{CO} , respectively, replaced by $K_{D\text{bulk}}$, $K_{D\text{max}}$, K_{DCO} [7] where $K_{D\text{bulk}}$ is the bulk dielectric constant where no reflection is assumed, $K_{DCO}(|k_z|, |k_y|)$ is the cutoff dielectric constant and $K_{D\text{max}}$ is a few times K_{DCO} .

4. A sub-problem: optimization of the coupling through an evanescent layer to a homogeneous propagating medium

We consider a uniform plasma of density N facing the antenna array at a constant distance plasma edge–antenna a (single-step profile: see figure 6). The results of a plasma density scan for the different toroidal phasing cases are shown in the figure. For each phasing the coupling goes through a significant maximum for a density N_{max} larger than the cutoff one N_{CO} but of the same order of magnitude. These results are obtained for the complete k_z, k_y spectrum excited by the antenna array.

An approximate analytic expression of this coupling optimum can be obtained by considering the behaviour of the most excited Fourier wave component characterized by $k_z = k_{z\text{M}}$ and $k_y = k_{y\text{M}}$. Solving the boundary conditions problem for this wave in region 1, the surface impedance ξ_0 obeys the relation

$$\xi_0 = \xi_v \{ \xi_1 + \xi_v \tanh(pa) \} / \{ \xi_v + \xi_1 \tanh(pa) \} \quad \text{with } p = (k_{z\text{M}}^2 + k_{y\text{M}}^2 - k_0^2)^{0.5}, \quad (4)$$

where ξ_v is the surface impedance of vacuum (without reflection) given by $\xi_v = -ip/(k_0^2 - k_z^2)$ and ξ_1 is the surface impedance of the uniform plasma or dielectric medium without reflection (≡single pass absorption) given by $\xi_1 = \xi_p = -i(-i\rho + \mu k_y)/k_\perp^2$ for plasma with $\rho = (k_\perp^2 - k_y^2)^{1/2}$ and by $\xi_1 = \xi_d = (k_{\perp d}^2 - k_y^2)^{1/2}/k_{\perp d}^2$ for dielectric with $k_{\perp d}^2 = k_0^2 K_D - k_z^2$. If the wave is propagating in the plasma (or dielectric) and evanescent in vacuum, ξ_1 is real and

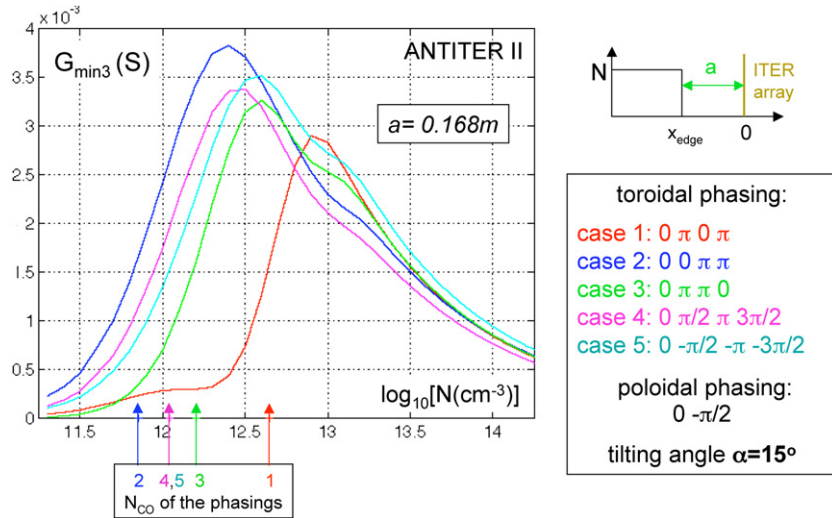


Figure 6. Evolution of the coupling performances to a uniform plasma at distance a of the ITER antenna array as a function of the plasma electron density N for the different toroidal phasing cases. The corresponding values of N_{CO} are indicated.

ξ_v is imaginary. In this condition the surface conductance $Re\{1/\xi_0^*(|k_{zM}|, k_{yM})\}$ has a strong maximum for $N = N_{\max}$ or $K_D = K_{D\max}$ fulfilling the condition $|\xi_1/\xi_v| = \tanh(pa)$.

In the limit $|k_{zM}|^2 \gg k_0^2$ and $k_{zM}^2 \gg k_{yM}^2$ these maximum values are given by

$$N_{\max} \cong N_{CO}\{1 + 1/(2\tanh^2(k_{zMA}))\} \quad \text{and} \quad K_{D\max} \cong K_{D,CO}\{1 + 1/\tanh^2(pa)\}, \quad (5)$$

respectively, for plasma and dielectric.

From equation (3) we have $G_{\min 3}(N_{\max}) \propto Re\{1/\xi_0^*(|k_{zM}|, k_{yM})\}_{\max}$ as long as the excitation function $\int \int_{\mathbb{R}} |E|^2 dk_z dk_y$ does not undergo a significant drop when a is decreasing (this occurs for $a < 5$ cm in the considered reference ITER case), while $Re\{1/\xi_0^*(|k_{zM}|, k_{yM})\}_{\max} = 1/|\xi_v \sinh(2pa)|$. This relation becomes in the same limit $|k_{zM}|^2 \gg k_0^2$ and $k_{zM}^2 \gg k_{yM}^2$:

$$Re\{1/\xi_0^*(|k_{zM}|, k_{yM})\}_{\max} \cong k_{zM}/[\sinh(2k_{zMA})]. \quad (6)$$

The maximum coupling is thus a strongly decreasing function of the distance antenna–plasma edge a : it decreases as $1/(2a)$ for $|k_{zMA}| \ll 1$ and as $2|k_{zM}| \exp(-2|k_{zMA}|)$ for $|k_{zMA}| \gg 1$.

5. The impact of regions 1 and 2 of the plasma profile

5.1. Influence of the presence of edge density N_{edge} lower than N_{CO} on the coupling

Figure 7 illustrates the influence of the layer of density $N < N_{CO}$ and of the N_{bulk} –antenna distance on the coupling of the different considered phasing cases. The coupling is expressed by the effective minimum conductance $G_{\min 3}$. We consider the cases of two distances N_{bulk} –antenna, i.e. $|x_{\text{bulk}} - x_{\text{antenna}}| = 21$ and 25 cm, and for each case we interrupt the exponentially decaying profile (with $l_{\text{SOL}} = 2.4$ cm) at a variable position of x_{edge} . The positions of $|x_{\text{bulk}} - x_{\text{edge}}| = |x_{\text{bulk}} - x_{CO}|$ with x_{CO} corresponding to $N = N_{CO}(|k_{zM}|, k_{yM})$ for the phasing cases 1 and 2 are indicated in the figure. At these positions the region 1 of the most excited Fourier wave component of each phasing case is depleted of plasma. When $|x_{\text{bulk}} - x_{\text{edge}}|$

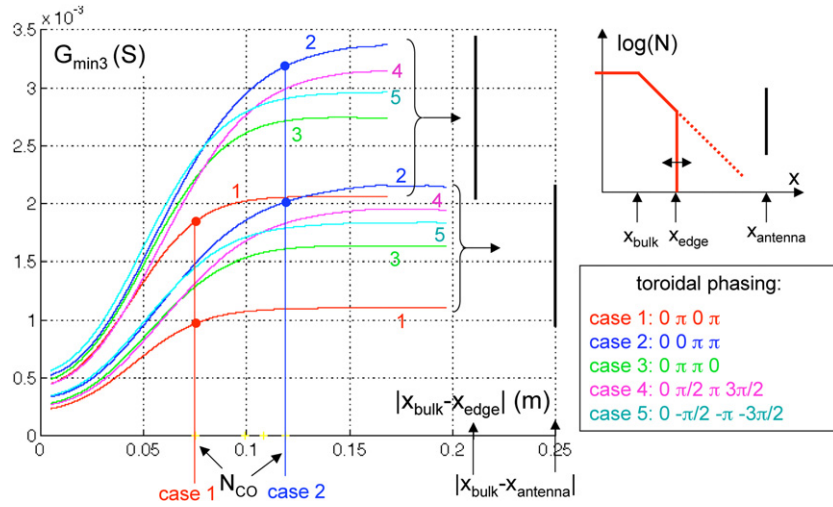


Figure 7. Evolution of the coupling expressed by $G_{\min 3}$ to an exponentially decaying profile interrupted at a variable x_{edge} position (the region $x_{\text{edge}}-x_{\text{antenna}}$ being replaced by vacuum). This is done for two different distances $N_{\text{bulk}}-\text{antenna}$.

increases above $|x_{\text{bulk}} - x_{\text{CO}}|$ a larger part of the profile below cutoff is retained. The figure shows the modest influence of the presence of plasma density in region 1 ($N < N_{\text{CO}}$) on the coupling to the plasma bulk for a given cutoff–antenna distance even if the contribution of the complete k_z, k_y spectrum is taken into account. On the other hand, cutting a part of the profile above cutoff (for $|x_{\text{bulk}} - x_{\text{edge}}| < |x_{\text{bulk}} - x_{\text{CO}}|$) or increasing the width of the vacuum layer by moving back the antenna produces a substantial decrease in coupling

5.2. Effect of variation of thickness of region 2 (distance $N_{\max}-N_{\text{CO}}$) and comparison with the same variation of the one of region 1

Figure 8 illustrates the negative effect of the distance between N_{\max} and N_{CO} in the density profile: (i) we consider for phasing case 1 a density profile with a fixed distance cutoff position $x_{\text{CO}}-\text{antenna}$ of 0.155 m as for the reference profile and a fixed value of $N_{\text{bulk}} = 8 \times 10^{18} \text{ m}^{-3} \cong N_{\max}$ of this phasing. Between N_{CO} and the antenna we consider an exponential decaying profile characterized by $l_{\text{SOL}2} = 0.1 \text{ cm}$ and between N_{CO} and N_{\max} we vary the decay length l_{SOL} from 0.1 to 5.1 cm (see figure 8(a)). As a result we shift the position x_{\max} of N_{\max} up to 3 cm farther from the antenna than the x_{CO} position. The corresponding evolution of $G_{\min 3}$ versus l_{SOL} as given in figure 8(b) shows a decrease in coupling as the distance $|x_{\max} - x_{\text{CO}}|$ increases. (ii) We perform the same computation using the same profiles but with x_{CO} shifted 3 cm farther from the antenna. With $l_{\text{SOL}} = 0.1 \text{ cm}$ the position of N_{\max} is the same as in the first case with $l_{\text{SOL}} = 5.1 \text{ cm}$ but the decrease in coupling is larger (37% instead of 15%). This again shows the importance of bringing the cutoff as close as possible to the antenna. A further increase in coupling requires bringing the position of N_{\max} close to that of N_{CO} . Note that the ratios of $G_{\min 3}$ for the two steepest profiles corresponding to $l_{\text{SOL}} = 0.1 \text{ cm}$ are in close agreement with the one expected from relation (6) (with $|k_z M| = 7.5 \text{ m}^{-1}$ and $a = 0.155 \text{ m}$ or 0.185 m).

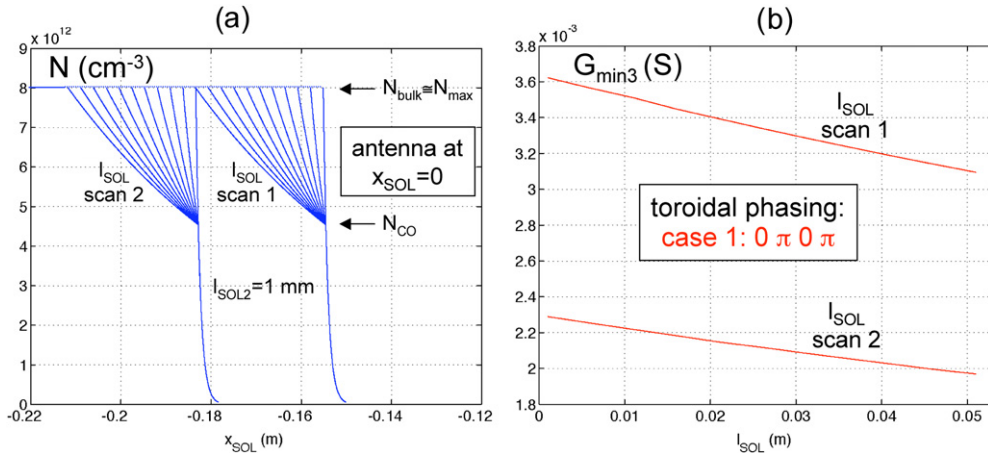


Figure 8. (a) Considered density profiles with variable distance $N_{\text{CO}} - N_{\max}$ for two distances $N_{\text{CO}} - \text{antenna}$ (toroidal phasing case 1). (b) Corresponding evolution of $G_{\min 3}$ as a function of the distance $N_{\max} - N_{\text{CO}}$ set by l_{SOL} .

6. Effect of a density gradient in a region of wave propagation

Here, the effect of a density gradient is studied in a region where the fast wave is propagating ($N > N_{\text{CO}}$). We first show the result on coupling when a gradient scan is performed starting from a location with density $N_{\text{TO}} > N_{\text{CO}}$. The most salient feature is the appearance of coupling oscillations. The underlying wave reflection mechanism is then studied in detail as a second analytical sub-problem in section 6.2.

6.1. Gradient scan

We consider a plasma profile with two density decay lengths, the first $l_{\text{SOL}1}$ between N_{bulk} and a density N_{TO} ($N_{\text{TO}} > N_{\text{CO}}$) and the second $l_{\text{SOL}2}$ for $N < N_{\text{TO}}$. For the example shown in figure 9 we choose $N_{\text{TO}} \approx N_{\max}$ of case 1 of toroidal phasing, a constant $l_{\text{SOL}2}$ value ($l_{\text{SOL}2} = 2.4 \text{ cm}$) and we make a scan of $l_{\text{SOL}1}$ values between 0.5 mm and 20 cm for three different bulk densities N_{bulk} as shown in figure 9(a). Note that $l_{\text{SOL}1} = 2.4 \text{ cm}$ corresponds to the reference profile. We consider the phasing cases 1 and 2 corresponding, respectively, to the highest and the lowest value of $|k_z M|$. As $N_{\text{TO}} > N_{\text{CO}}$ the $N_{\text{CO}} - \text{antenna}$ distance for these two considered phasing cases remains constant. Figure 9(b) reveals the existence of a series of $G_{\min 3}$ oscillations as a function of $l_{\text{SOL}1}$. Our analysis shows that (i) the oscillation period is a function of N_{bulk} , (ii) the coupling is low before the first maximum, (iii) the amplitude of this first maximum decreases when N_{bulk} increases and (iv) the asymptotic coupling for large $l_{\text{SOL}1}$ is independent of N_{bulk} and roughly corresponds to the coupling to a uniform plasma of density N_{TO} at the same $N_{\text{CO}} - \text{antenna}$ distance when the position of N_{TO} is close to that of N_{CO} .

6.2. A second sub-problem: wave reflection due to the density or dielectric constant gradient

To fully quantify the reflection in the plasma density or dielectric constant gradient region (from x_{bulk} to x_{TO}) analytically we consider that the plasma or dielectric constant profile is excited in $x = x$ by waves travelling either in an uniform plasma of density $N(x)$ (see figure 10) or in

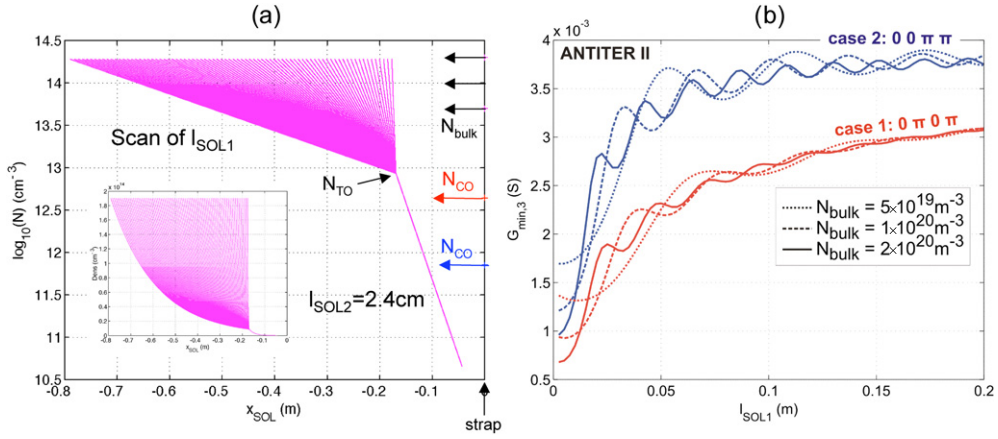


Figure 9. $G_{\min,3}$ as a function of the plasma electron density decay length $l_{\text{SOL}1}$ (between $N_{\text{TO}} \sim N_{\max, \text{case}1}$ and N_{bulk}) for fixed $l_{\text{SOL}2}$ (for $N < N_{\text{TO}}$). These N profiles considered for the $l_{\text{SOL}1}$ scan are shown in (a) on a logarithmic and a linear scale, whereas the evolution of $G_{\min,3}$ versus $l_{\text{SOL}1}$ is shown for two values of N_{bulk} and for phasing cases 1 and 2 in (b).

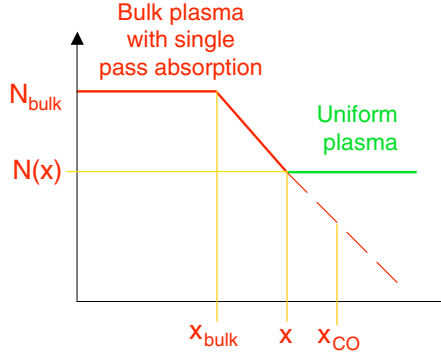


Figure 10. Density profile considered to evaluate the wave reflection due to the density gradient.

an homogeneous dielectric of constant $K_D(x)$ and we compute the reflection coefficient $\Gamma(x)$ seen in this uniform plasma or dielectric.

In the uniform plasma or dielectric we have $\omega B_z = Ae^{-i\rho x} + Be^{+i\rho x}$ where $\rho = (k_\perp^2 - k_y^2)^{1/2}$ for the plasma case and $\rho \equiv \rho_d = (k_{\perp d}^2 - k_y^2)^{1/2}$ for the dielectric.

In $x = x$ the surface impedance seen from the uniform plasma or dielectric is $\xi = E_y / \omega B_z$ due to the non-uniform plasma or dielectric terminated by the bulk plasma or dielectric with single pass absorption. The corresponding reflection coefficient is given

(i) for plasma by

$$\Gamma(x) = Be^{2i\rho x} / A = -(\xi - \xi_p) / (\xi + \xi_p + 2i\mu k_y / k_\perp^2), \quad (7)$$

where $\xi_p(x) = -i(-i\rho + \mu k_y) / k_\perp^2$ is the surface impedance of the uniform plasma of density $N(x)$ in the case of single pass absorption,

(ii) for dielectric by

$$\Gamma(x) = Be^{2i\rho x} / A = -(\xi - \xi_d) / (\xi + \xi_d), \quad (8)$$

where $\xi_d(x) = -\rho_d/k_{\perp d}^2$ is the surface impedance of the uniform dielectric with constant $K_D(x)$ without reflection (single pass absorption).

The surface impedance ξ can be obtained from the integration of a Riccati differential equation:

(i) for plasma:

$$\frac{d\xi}{dx} = -i(\rho/\xi_p)\{|\xi_p|^2 - \xi^2 + 2iIm(\xi_p)\xi\} \quad (9)$$

with $\xi = \xi_{\text{bulk}} = \xi_p(x_{\text{bulk}})$ as boundary condition in $x = x_{\text{bulk}}$.

(ii) for dielectric:

$$\frac{d\xi}{dx} = -i\rho_d(\xi_d - \xi^2/\xi_d) \quad (10)$$

with $\xi = \xi_{d,\text{bulk}}$ as boundary condition in $x = x_{\text{bulk}}$.

There is a complete analogy of this last differential equation with the one derived in the exact theory of wave propagation in tapered transmission lines: ξ corresponds to the taper input impedance in x , ξ_d is its local line characteristic impedance in $x = x$ (see [15, p 385]). The difference between the expressions for the plasma and the dielectric media results from the plasma gyrotropy. As in the tapered transmission line the oscillations of the reflection coefficient result from multiple reflections between the individual differential sections of the gradient region 3.

In the special case of a layer of uniform plasma density or dielectric constant of width $= \Delta a$, the variation of the surface impedance $\Delta\xi$ due to this layer is given by

(i) for plasma

$$\Delta\xi = -i\tan(\rho\Delta a)\{|\xi_p|^2 - \xi^2 + 2iIm(\xi_p)\xi\}/\{\xi_p - i(\xi - 2iIm(\xi_p))\tan(\rho\Delta a)\} \quad (11)$$

(ii) for dielectric

$$\Delta\xi = -i\tan(\rho_d\Delta a)(\xi_d^2 - \xi^2)/\{\xi_d^2 - i\xi\tan(\rho_d\Delta a)\}. \quad (12)$$

The surface impedance prior to the layer is ξ and after it $\xi + \Delta\xi$. These formulae allow us to compute the surface admittance of a multilayer plasma or dielectric (of application for modelling and multilayer dummy load; see also the appendix).

In figure 11(a) we display for case 1 ($0\pi 0\pi$) the reflection coefficient $|\Gamma(N = N_{\text{TO}})| = |\Gamma_{\text{NTO}}|$ as a function of the decay length l_{SOL1} between N_{bulk} and N_{TO} for different values of N_{bulk} ($0.2, 0.5, 1, 2 \times 10^{20} \text{ m}^{-3}$) and for $N_{\text{TO}} \cong N_{\text{max}} = 10^{18} \text{ m}^{-3}$. This computation is made for the Fourier spectrum wave component characterized by $k_{z\text{M}}$ and $k_{y\text{M}}$ of the considered case. The minima of reflection $|\Gamma_{\text{NTO}}|$ by the density gradient correspond to the maxima of coupling and are precisely given by (see figure 11(b))

$$\int_{N_{\text{bulk}}}^{N_{\text{TO}}} \rho(x) dx = n\pi \quad (n = 1, 2, 3 \dots) \\ \text{with } \rho^2(x) = k_{\perp}^2(x) - k_y^2 \quad \text{and} \quad N = N_{\text{bulk}} e^{-x/l_{\text{SOL1}}}. \quad (13)$$

To evaluate (13) we may use the approximate value $\rho^2(x) \approx (\omega^2/\omega_{ci}^2)(\omega_{pi}^2(x) - \omega_{pi}^2(x_{\text{CO}}))/c^2$ in the case of single species plasma. Relation (13) is also valid for the dielectric case if we, respectively, replace N_{bulk} , N_{TO} , $\rho^2(N)$, respectively, by $K_{D\text{bulk}}$, $K_{D\text{TO}}$ and $\rho_D^2(K_D)$. The reflection coefficient is large for l_{SOL1} smaller than its first minimum and its value for this first minimum increases with N_{bulk} . An approximate expression of l_{SOL1} corresponding to this first minimum for $k_y^2 \ll k_z^2$ and $k_0^2 \ll k_z^2$ is given by

$$(l_{\text{SOL1}})_{\text{M1}} = (\lambda_0/2)(\omega_{ci}/\omega_{pi})_{x=x_{\text{bulk}}} = (\lambda_A/2)_{x=x_{\text{bulk}}} \quad \text{with } \lambda_A = v_A/f \quad (14)$$

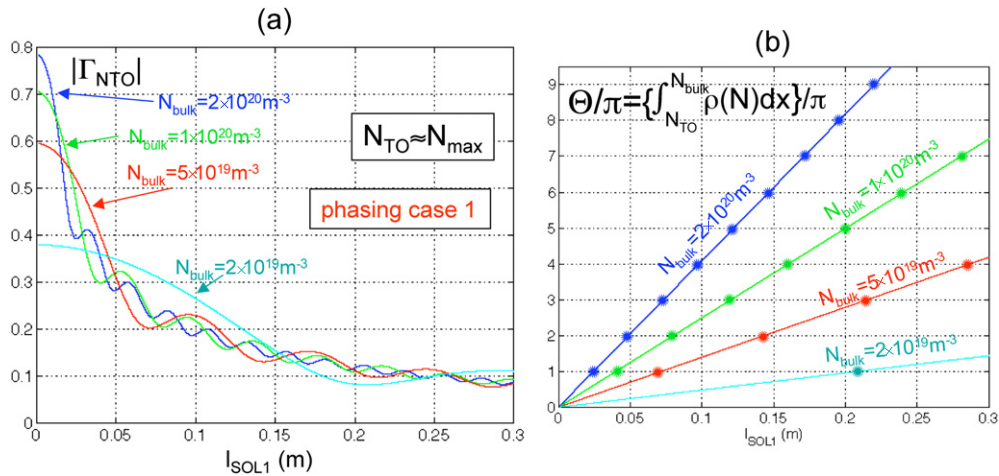


Figure 11. (a) Amplitude of reflection coefficient $|\Gamma_{NTO}|$ due to the density gradient as a function of l_{SOL1} for different values of N_{bulk} . (b) Corresponding evolution of the integral Θ of the radial propagation constant ρ between N_{TO} and N_{bulk} .

for plasma (λ_0 is the vacuum wavelength and v_A is the Alfvén velocity) and by

$$(l_{SOL1})_{M1} = \lambda_0 / \{2\sqrt{K_D}(x = x_{bulk})\} \quad (15)$$

for dielectric. The minima of $|\Gamma_{NTO}|$ for $N_{TO} \cong N_{max}$ and $k_z = k_{zM}$, $k_y = k_{yM}$ correspond to good approximation to the maxima of G_{min3} in the full wave spectrum calculation.

7. The combined effect of changing the magnitude of the density gradient up to the bulk and the location from where it starts

We consider the same far-edge density profile as for the reference case ($l_{SOL2} = 2.4$ cm) and the same bulk density ($N_{bulk} = 10^{20} m^{-3}$) but for different values of N_{TO} we scan the gradient between N_{TO} and N_{bulk} by varying l_{SOL1} from 0.5 mm to 20 cm as shown in figure 12(a). This is done for the toroidal phasing cases 1 and 2. The antenna– N_{CO} distance is always the same for case 2; for case 1 it is closer or farther depending if $l_{SOL1} <$ or $>$ 2.4 cm. Note that N_{TO} for some phasings is even chosen below the corresponding cutoff density. The results of the computation (with full k_z , k_y wave spectrum), giving G_{min3} as a function of l_{SOL1} for the different N_{TO} values, are shown in figure 12(b). For $l_{SOL1} = 2.4$ cm we have the conditions of the reference profile. We also see that the optimum asymptotic coupling for large l_{SOL1} value occurs when N_{TO} is close to the N_{max} of the considered case, i.e. $\sim 3 \times 10^{18} m^{-3}$ for case 2 (0 π π) and $\sim 8 \times 10^{18} m^{-3}$ for case 1 (0 π 0 π). The coupling is low before the first maximum and the reference profile as shown in the figure is below it for all phasing cases but not too far from it principally for case 2 (lowest $|k_{zM}|$).

We can conclude sections 4–7 by stating that coupling optimization for a given cutoff–antenna distance requires bringing N_{max} as close as possible to N_{CO} and having a gradient length as large as possible and at least equal or above the value leading to the first maximum of coupling. Larger coupling values can be obtained by edge selective resonances requiring dedicated plasma edge profile as studied in the next section.

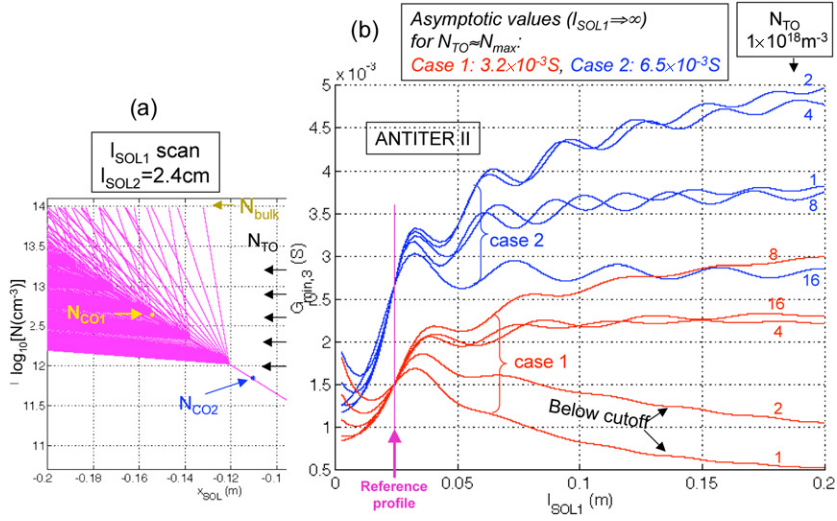


Figure 12. (a) Density profiles used for the density decay length l_{SOL1} scan between N_{bulk} and N_{TO} for different values of N_{TO} . (b) Corresponding evolution of $G_{\min 3}$ versus l_{SOL1} for the same N_{TO} values, indicated in units of 10^{18} m^{-3} .

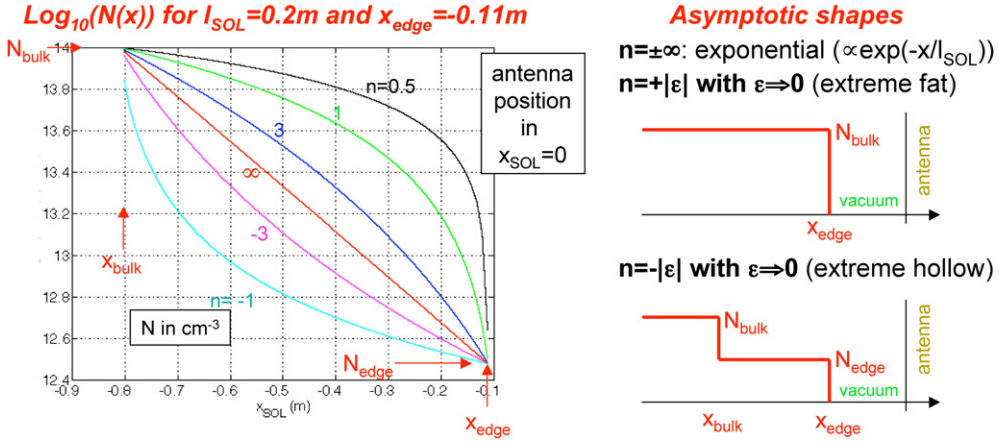


Figure 13. Display of the edge density profiles used to describe the departure with respect to an exponentially decaying one ($|n| = \infty$). The asymptotic shapes for $n \Rightarrow 0$ are shown on the rhs.

8. Effect of departures from an exponentially decaying profile

As exponential decay is at best an approximation, it is worthwhile to also study variations thereon. To this end, we choose an edge density profile

$$N(x) = N_{\text{bulk}}(1 - |x|/\Lambda_n)^n \quad (16)$$

with $\Lambda_n = x_{\text{pr}}/(1 - (N_{\text{edge}}/N_{\text{bulk}})^{1/n})$, $x_{\text{pr}} = |x_{\text{bulk}} - x_{\text{edge}}| = l_{\text{SOL}} \ln(N_{\text{bulk}}/N_{\text{edge}})$ and $0 < x < x_{\text{pr}}$.

This function has for a limit the exponential decaying profile $N(x) = N_{\text{bulk}} \exp(-x/l_{\text{SOL}})$ when $n \Rightarrow \pm\infty$, is more hollow than this one when $n < 0$ and fatter when $n > 0$ as illustrated in figure 13. The profile length $x_{\text{pr}} = |x_{\text{bulk}} - x_{\text{edge}}| = l_{\text{SOL}} \ln(N_{\text{bulk}}/N_{\text{edge}})$ is the same

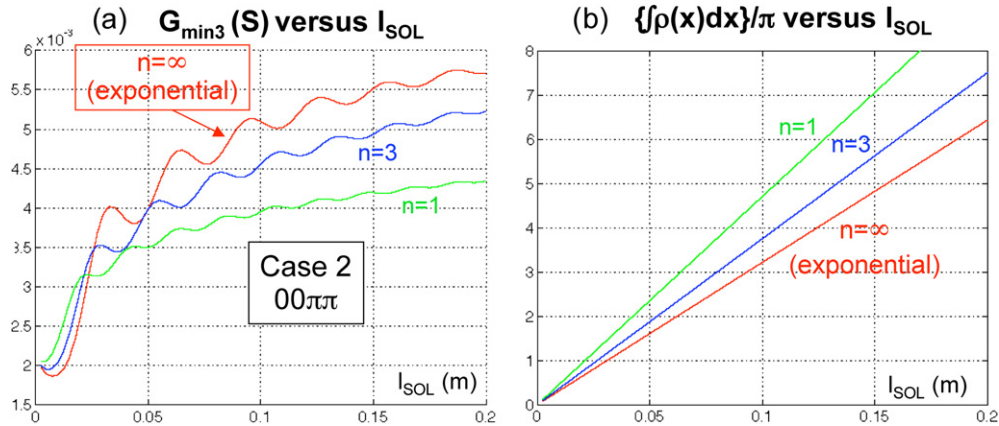


Figure 14. (a) Evolution of $G_{\min 3}$ versus the length l_{SOL} (= the decay length for $|n| = \infty$) for positive values of n (fat edge profiles), $N_{\text{bulk}} = 10^{20} \text{ m}^{-3}$, $N_{\text{edge}} = 3 \times 10^{18} \text{ m}^{-3}$, $x_{\text{edge}} = 0.11 \text{ m}$ and phasing case 2. (b) Corresponding evolution of the integral of the radial propagation constant ρ between x_{edge} and x_{bulk} .

whatever the value of n and we use l_{SOL} as normalized inhomogeneous profile length. l_{SOL} corresponds to the usual density decay length when $n \Rightarrow \pm\infty$. The value of n characterizes the non-exponentially decaying profiles. The asymptotic shapes are also displayed in figure 13: (i) for $n = +|\varepsilon|$ with $\varepsilon \Rightarrow 0$ we have the extreme fat profile corresponding to the single-step homogeneous profile studied in section 4, (ii) for $n = -|\varepsilon|$ with $\varepsilon \Rightarrow 0$ we have the extreme hollow profile corresponding to the two-step density profile. For $n = \pm\infty$ we recover the exponentially decaying profile $\propto \exp(-x/l_{\text{SOL}})$.

8.1. Fat profiles ($\infty > n > 0$)

In this case $G_{\min 3}$ displays the same behaviour versus l_{SOL} (i.e. the normalized width of the gradient layer) for fat profiles as for the exponential one, but with smaller and smaller oscillation amplitude when n decreases as shown in figure 14(a). The position of maxima is still given by $\int \rho(x) dx \cong n\pi$ (see figure 14(b)). The asymptotic value of $G_{\min 3}$ for $n \Rightarrow 0$ is the one obtained if N_{bulk} extended up to x_{edge} .

8.2. Hollow profiles ($-\infty < n < 0$)

We have also the same behaviour versus l_{SOL} as for the exponential profile, but with larger oscillation amplitude as appearing in figure 15. They become much larger when $n \Rightarrow 0$. The position of maxima is still given by $\int \rho(x) dx \cong n\pi$ with some shift towards $n\pi - \pi/2$ when $n \Rightarrow 0$.

Therefore if the density gradient region of the plasma edge is more hollow than the exponential one ($n < 0$ curves in figure 13) the $G_{\min 3}$ oscillations become larger and larger when $n \Rightarrow 0$ leading to strong coupling resonances. They correspond in the limit $n = -|\varepsilon|$ with $\varepsilon \Rightarrow 0$ to the eigenmodes of the system shown in figure 15. They are approximately solutions of

$$\tan(\rho b)/\rho = -\tanh(k_{zM}a)/k_{zM}, \quad (17)$$

where b is the width of the plasma step as indicated in figure 16. Figure 17(a) shows the two first resonances of $G_{\min 3}$ for an extreme case (case 2 (0 0 $\pi\pi$) with $n = -0.2$). The fields

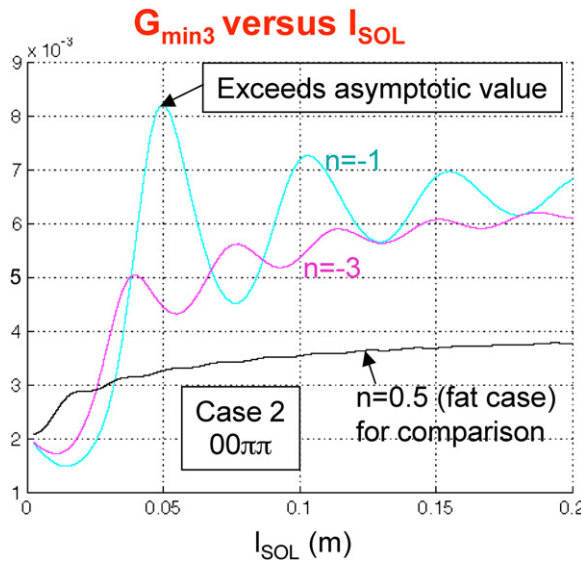


Figure 15. The same as figure 14(a) but for hollow profiles and comparison with the result for a very fat profile.

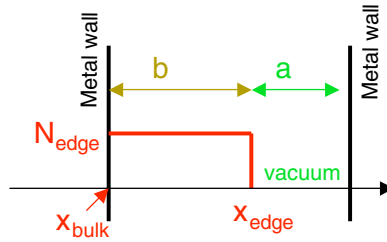


Figure 16. Single-step plasma profile between two metal walls.

show a resonant structure in the domain including the hollow profile and the region below cutoff up to the antenna as illustrated in figure 17(b) for the first resonance condition and in figure 17(c) for the second one. The (k_{zM}, k_{yM}) wave field behaviour for the two first minima is also displayed for comparison. The curves labelled ‘P’ show the normalized field $|E_y(x)|$ from the antenna ($x = 0$) up to the bulk plasma (at $x = x_{\text{bulk}}$ with $N_{\text{bulk}} = 10^{20} \text{ m}^{-3}$). For comparison the curves labelled ‘vac’ show the corresponding field amplitude for the vacuum case (no plasma) $E_y \propto \exp(px)$ and the curve labelled ‘M’ also corresponds to the vacuum case but with a metal plate in $x = x_{\text{bulk}}$ replacing the plasma bulk edge. In this case we have $E_y \propto \sinh\{p(x - x_{\text{bulk}})\}/\sinh\{-px_{\text{bulk}}\}$ with $p = (k_{zM}^2 + k_{yM}^2 - k_0^2)^{1/2}$. The occurrence of the edge resonances is very sensitive to the values of k_{zM} and a , which must satisfy the resonance condition (approximately given by (17)). The selectivity in k_{zM} appears in the contour plot of the surface conductivity $\text{Re}(1/\xi_0)$ in front of the array shown in figure 18(a). For the considered profile parameters a sharp maximum takes place for $|k_z| = 7.5 \text{ m}^{-1}$ and $k_y \cong 2 \text{ m}^{-1}$ and leads to a coupling resonance for phasing case 1. The sharp coupling is moving towards the lower values of $|k_z|$ when the hollow layer thickness x_{pr} is decreasing as shown by the cut of the surface $\text{Re}(1/\xi_0)$ given in figure 18(b). Therefore, the other phasing cases successively have coupling resonance when x_{pr} is decreasing. Figure 18(a) shows also the location of coaxial and

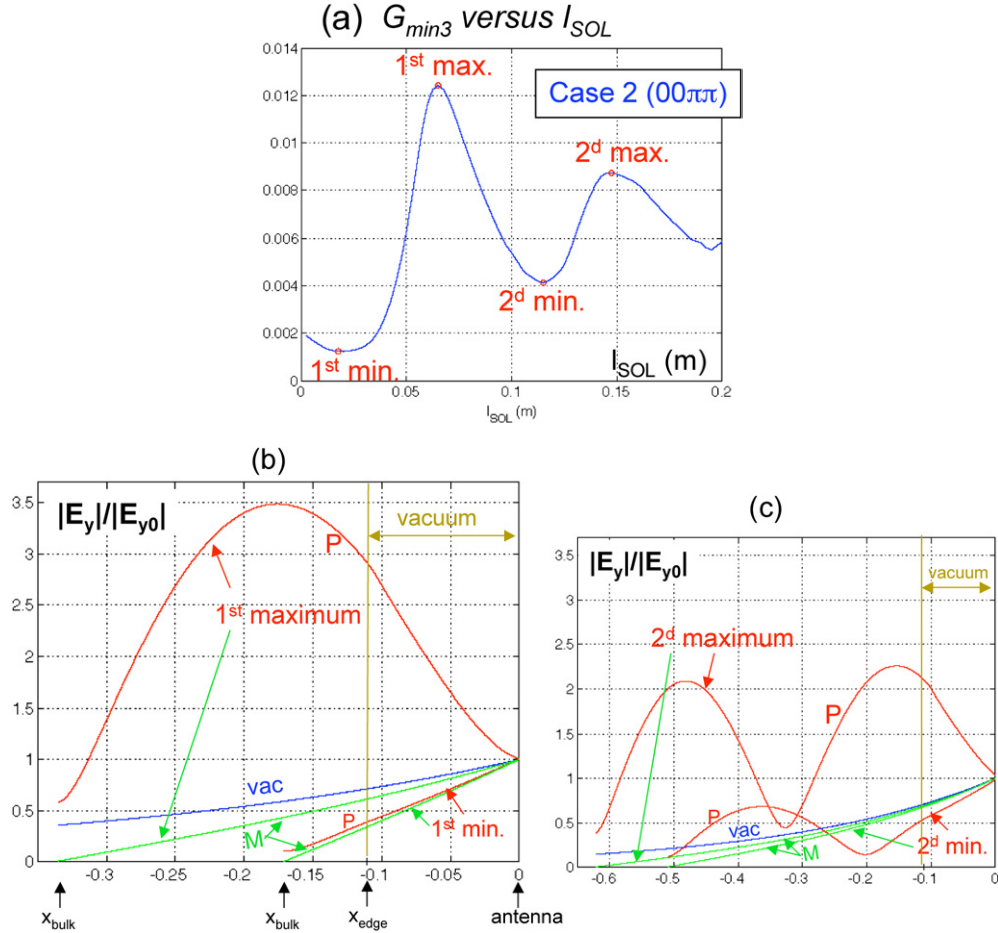


Figure 17. (a) Two first resonances of $G_{\min 3}$ versus the length l_{SOL} for a very hollow edge plasma profile ($n = -0.2$), $N_{\text{bulk}} = 10^{20} \text{ m}^{-3}$, $N_{\text{edge}} = 3 \times 10^{18} \text{ m}^{-3}$, $x_{\text{edge}} = 0.11 \text{ m}$ and phasing case 2; (b) evolution between the wall of the corresponding $(k_z M, k_y M)$ wave electric field amplitude $|E_y|$ normalized with respect to $|E_{y0}| \equiv |E_y(x = 0)|$ for the first maximum and first minimum of coupling ('P' curves). The corresponding evolution in the absence of plasma in (i) vacuum (curves 'VAC') or in vacuum up to a metal wall at x_{bulk} (curves 'M') is given; (c) The same as figure 17(b) but for the second minimum and maximum of figure 17(a).

surface modes, which have no significant excitation by the considered array phasing cases: the coaxial modes need a low k_z ($\sim < k_0$) excitation as in the monopole (0 0 0) toroidal phasing and the surface modes a large k_y one.

Note that the coupling for dielectric medium with hollow K_D profile shows similar behaviour and relation (17) remains valid if we replace ρ by ρ_d . The cases of multilayer plasma (academic or approximate modelling) or dielectric profiles approaching an inhomogeneous one are discussed in the appendix.

9. Applications to the ITER case

To illustrate the coupling physics described in the preceding sections we will start by showing how slight modifications of the reference profile can strongly improve the coupling

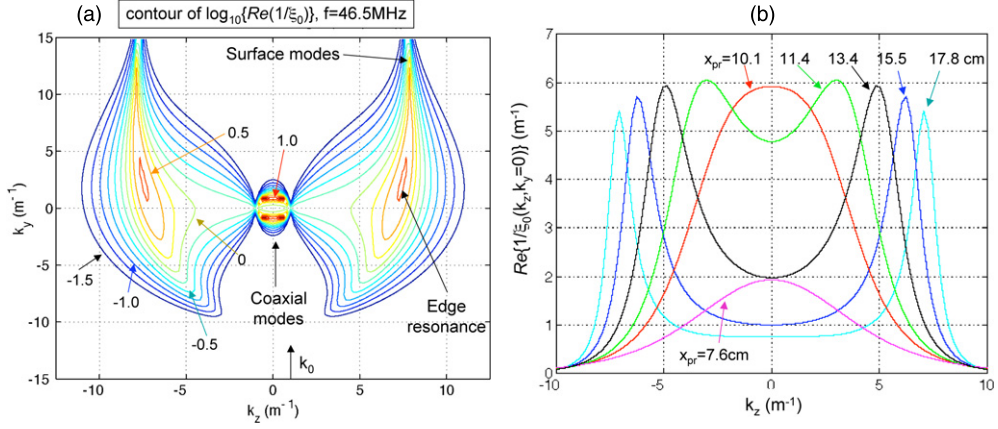


Figure 18. (a) Contour plot in the k_z , k_y plane of the surface conductance in front of the array for $N_{\text{bulk}} = 10^{20} \text{ m}^{-3}$, $N_{\text{edge}} = 8 \times 10^{18} \text{ m}^{-3}$, $n = -0.2$ with $l_{\text{SOL}} = 0.0703 \text{ m}$, i.e. $x_{\text{pr}} = 17.8 \text{ cm}$ (the edge resonance condition occurs for phasing case 1 characterized by $|k_{zM}| = 7.5 \text{ m}^{-1}$ and $k_{yM} = 1.25 \text{ m}^{-1}$). (b) Evolution of the surface conductance for $k_y = 0$ as a function of k_z for different values of the width of the hollow profile x_{pr} (the values of N_{bulk} and N_{edge} are the same as for figure 18(a)).

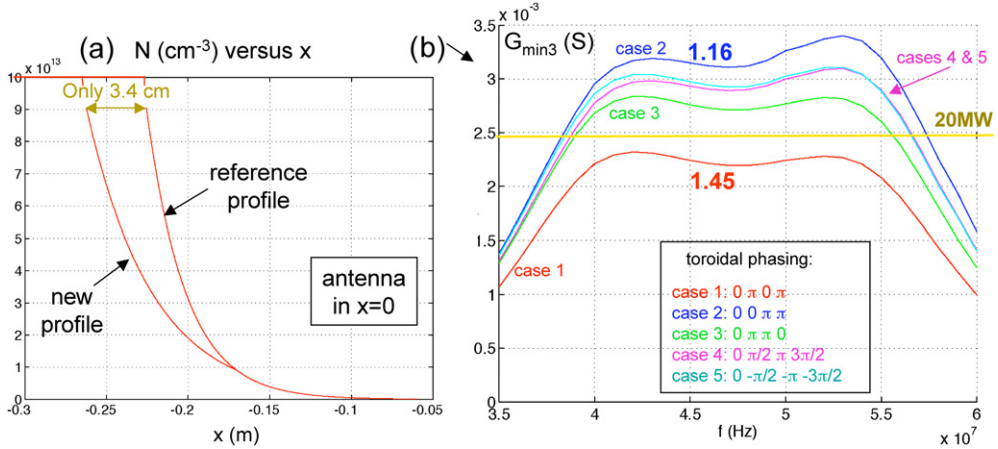


Figure 19. Effect of small modification of the reference profile to optimize phasing case 1. (a) Modified profile compared with the reference one; (b) $G_{\min 3}$ versus f for the different phasing cases. The improvement factor with respect to the reference case (figure 5(a)) at $f = 46 \text{ MHz}$ for phasing cases 1 and 2 is indicated in bold.

performances. We will continue by comparing the effect of larger modifications of the reference profile including the ones corresponding to the limiting cases considered for ITER. Finally ‘academic’ modifications allowing extreme coupling performances are considered.

9.1. Slight profile modifications

- (i) In figure 19 we show the coupling increase by increasing l_{SOL1} from 2.4 to 4 cm for $N > N_{\text{TO}} = 8 \times 10^{18} \text{ m}^{-3}$. This is done with the same far-edge density profile as the reference case ($l_{\text{SOL2}} = 2.4 \text{ cm}$) and the same $N_{\text{bulk}} = 10^{20} \text{ m}^{-3}$. The N_{CO} -antenna distances

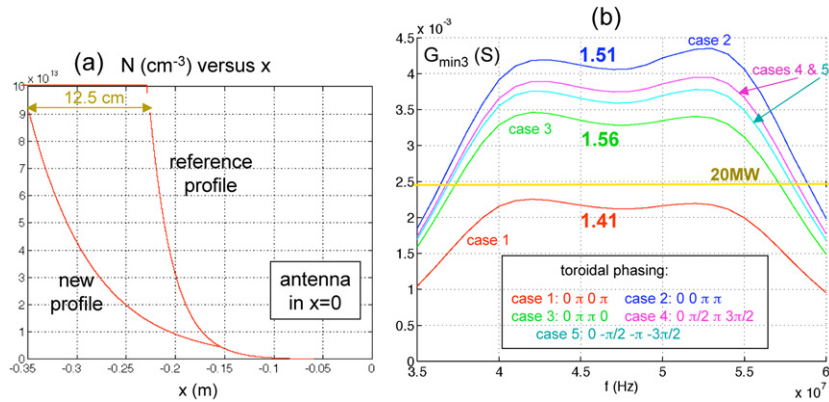


Figure 20. Effect of modification of the reference profile to optimize phasing case 2. (a) Modified profile compared with the reference one. (b) $G_{\min 3}$ versus f for the different phasing cases. The improvement factor at $f = 46$ MHz for phasing cases 1, 2 and 3 is indicated in bold.

for the different phasings are unchanged with respect to the reference case but the value of l_{SOL1} and $N_{\text{TO}} = 8 \times 10^{18} \text{ m}^{-3}$ corresponds to the optimum value of the first maximum of coupling for phasing case 1 ($0 \pi 0 \pi$) (see figure 12(b)). This leads to a coupling gain of 45% for case 1 as shown in the figure and also to a significant gain for the other phasing cases. The profile modification corresponds to an increase in the total density decay length of only 3.4 cm as shown in figure 19.

(ii) In figure 20 we show the effect of a similar optimization for phasing case 2 ($0 0 \pi \pi$). Here still with the same far-edge density profile as for the reference case ($l_{\text{SOL2}} = 2.4$ cm) and the same $N_{\text{bulk}} = 1 \times 10^{20} \text{ m}^{-3}$ we choose $l_{\text{SOL1}} = 6.5$ cm and $N_{\text{TO}} = 4 \times 10^{18} \text{ m}^{-3}$ in order to have the conditions of the best second coupling maximum for case 2 as shown in figure 12(b). It corresponds to a coupling gain of 51% with respect to the reference case without modifying the N_{CO} -antenna distance. A similar gain is observed for the other phasing cases because for the same N_{CO} -antenna (or about the same distance for case 1) the value of l_{SOL1} is increased. The gain of case 1 is nevertheless lower than in the preceding case of figure 19 where N_{TO} was just chosen to optimize this case. The profile modification corresponds to an increase of 12.5 cm of the total density decay length as shown in figure 20(a).

9.2. Larger profile modifications: extreme profile cases considered for ITER

Figure 21(a) shows the reference profile compared (i) with a profile ‘H’ characterized by a large l_{SOL} and an edge density close to N_{max} of toroidal phasing case 1 and (ii) with a profile ‘L’ having about the same l_{SOL1} as the reference one and a larger l_{SOL2} starting from a density lower than N_{CO} of phasing case 2. These profiles ‘H’ and ‘L’ are approximations of the ITER edge plasma profiles ‘2010 high’ and ‘2010 low’, which are considered for coupling as the most optimistic and the most pessimistic ones [16].

For the profile ‘H’ we have the N_{CO} -antenna distance much shorter for all phasing cases than for the reference case. The edge density $N_{\text{edge}} = 8 \times 10^{18} \text{ m}^{-3}$ is close to N_{max} of phasing case 1 and furthermore the l_{SOL} values are large. We are then near the optimum coupling conditions for case 1 which has a coupling increase of about 840% with respect to the reference case as shown in figure 21(b). The coupling hierarchy between the phasing cases is reversed with respect to the reference case as dictated by the coupling conditions described

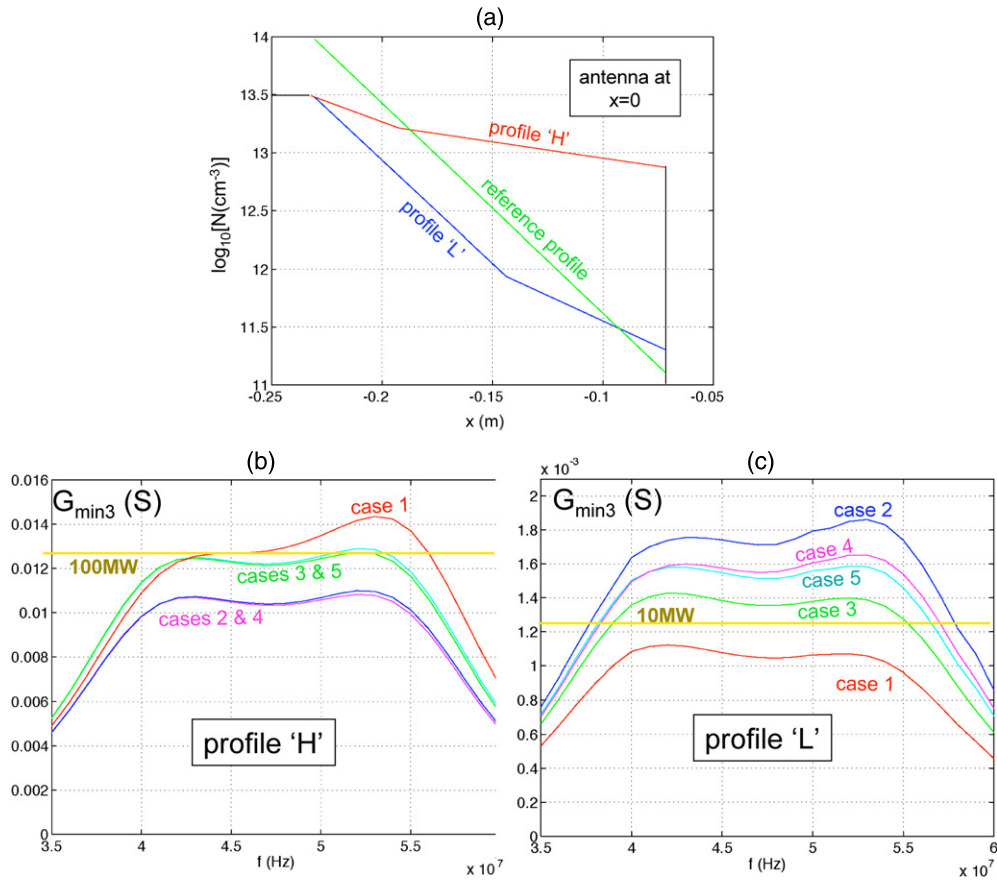


Figure 21. (a) Plasma edge profiles ‘L’ and ‘H’ as compared with the reference one; (b) and (c) $G_{\min 3}$ of the different phasing cases versus frequency for the ‘H’ and ‘L’ profiles.

in section 4 and illustrated in figure 6. Indeed figure 6 shows that phasing case 1 is at N_{\max} whereas cases 2 and 4 are farther from the optimum coupling for $N_{\text{edge}} = 8 \times 10^{18} \text{ m}^{-3}$. This is well reflected in the results shown in figure 21(b).

For the profile ‘L’ the N_{CO} -antenna distance for all phasing cases is increased by about 2.5 cm with respect to the reference case. This leads to a coupling decrease of $\approx 35\%$ for all cases as seen when comparing figures 21(c) and 5(a).

9.3. Extreme academic profiles

- (i) For the first profile we take the same N_{CO} -antenna distance $a = 11 \text{ cm}$ and same $N_{\text{bulk}} = 10^{20} \text{ m}^{-3}$ as in the reference case for phasing case 2 (see profiles in figure 22(a)) and we try to optimize the coupling of this phasing case by acting on l_{SOL1} and l_{SOL2} with $N_{\text{TO}} = 3 \times 10^{18} \text{ m}^{-3} \cong N_{\max}$. In figure 22(b) we show the dependence of the coupling on l_{SOL1} for different values of l_{SOL2} . For $l_{\text{SOL1}} = 0.4 \text{ m}$ we are close to the maximum of coupling and as discussed in section 5.2 the best value of l_{SOL2} is the lowest one even if we suppress the part of the density profile with $N < N_{\text{CO}}$. Figures 22(c) and (d) show the resulting effect on all phasing cases when we take $l_{\text{SOL1}} = 0.4 \text{ m}$ with $l_{\text{SOL2}} = 2.4 \text{ cm}$ (as in the reference case) or 0.5 cm (see figure 22(b)).

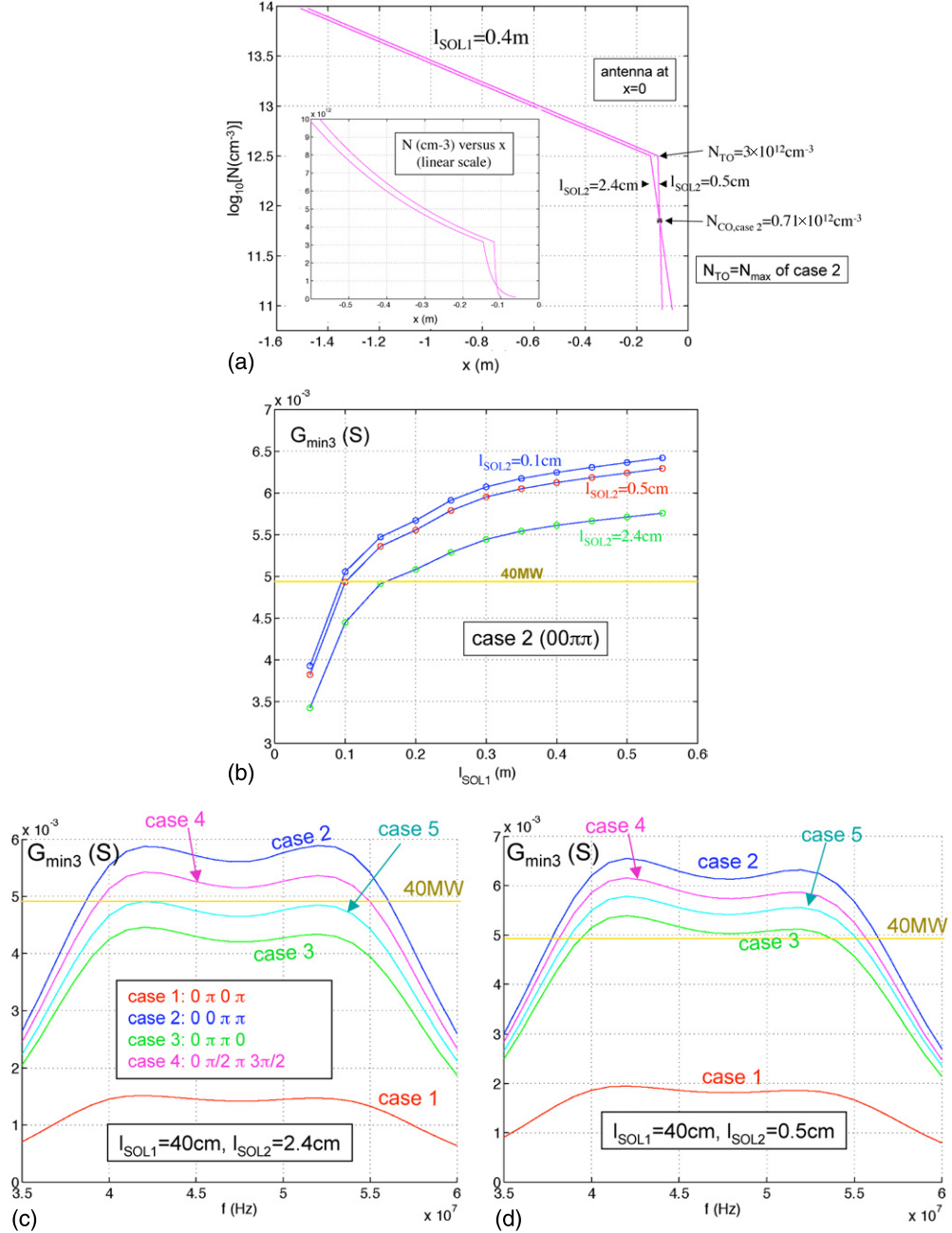


Figure 22. (a) Extreme edge profile for coupling optimization at the same distance N_{CO} -antenna as for the reference one; (b) $G_{\min 3}$ dependence on $l_{\text{SOL}1}$ for $f = 46.5\text{MHz}$ and different values of $l_{\text{SOL}2}$; (c) and (d) $G_{\min 3}$ versus frequency for the different phasing cases for the two profiles of figure 22(a).

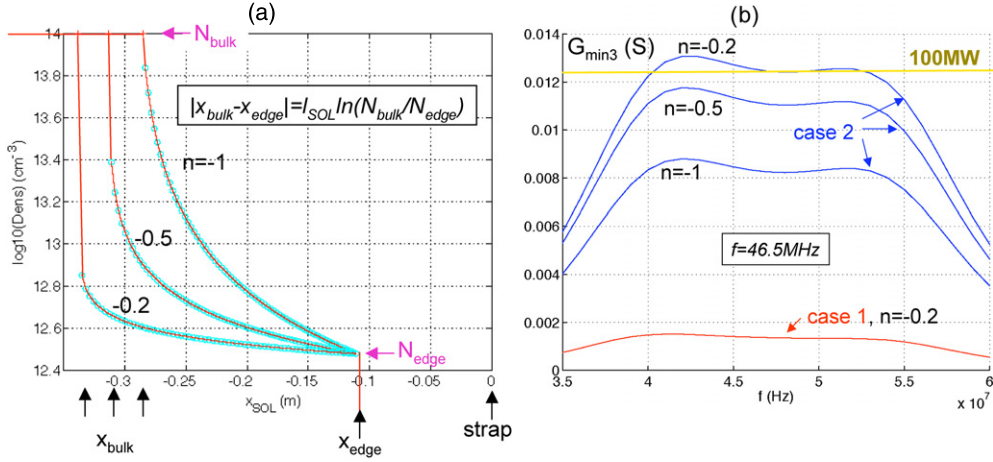


Figure 23. (a) Hollow edge profiles leading to large coupling resonance for phasing case 2; (b) $G_{\min 3}$ as a function of frequency for the profiles of figure 23(a) and phasing case 2. The result for phasing case 1 with the same $n = -0.2$ profile is added for comparison.

A large coupling improvement also occurs for the other phasing cases except for case 1. The competing effects of the larger l_{SOL1} value and the larger distances N_{CO} -antenna and $N_{\max} - N_{\text{CO}}$ for the different phasing cases can explain this.

(ii) For the second extreme case we consider the edge resonance produced by hollow profiles to maximize the coupling of phasing case 2 ($0 0 \pi \pi$) with still the same N_{CO} -antenna distance as for the reference profile. We choose $N_{\text{edge}} = 3 \times 10^{18} \text{ m}^{-3}$, $N_{\text{bulk}} = 10^{20} \text{ m}^{-3}$ with the hollow profile index defined in (16) $n = -0.2, -0.5, -1$ in order to excite the first edge resonance discussed in section 8.2. The corresponding equivalent $l_{\text{sol}} = 0.065, 0.058, 0.05 \text{ m}$ corresponding to $x_{\text{pr}} = |x_{\text{bulk}} - x_{\text{edge}}| = l_{\text{SOL}} \ln(N_{\text{bulk}}/N_{\text{edge}})$ equal, respectively, to 0.23, 0.20 and 0.175 m (see figure 23(a)). Figure 23(b) shows the very large coupling improvement for the same N_{CO} -antenna distance obtained thanks to this edge resonance, the optimum occurring when the profile becomes close to a two-step profile. Note that the value of x_{pr} is critical and depends also on the phasing: as shown in figure 23(a) the values of x_{pr} and n leading to the resonance of phasing case 2 do not improve the coupling for another phasing case with respect to the reference case. In contrast: for $n = -0.2$ and $x_{\text{pr}} = 0.23 \text{ m}$ the $G_{\min 3}$ improvement at mid-band with respect to the reference profile is 4.65 for case 2 and only 0.91 for case 1.

10. Conclusions

We have shown that the coupling of rf power by an ICRH antenna to a high-density plasma region N_{bulk} where almost total absorption occurs through an inhomogeneous edge plasma layer depends on the following parameters of the plasma shape: (i) distance between the cutoff density N_{CO} and antenna (critical), (ii) distance between density N_{\max} (equal to several times N_{CO}) and N_{CO} and (iii) density gradient between N_{\max} and N_{bulk} . The N_{CO} and N_{\max} values correspond to the wavenumbers $|k_{z\text{M}}|, k_{y\text{M}}$ predominantly excited by the phasing of the antenna array.

The first point (i) is well known because it corresponds to the length of wave evanescence. The second point (ii) is determined by the physics of antenna coupling to a propagating

region through an evanescent one: for a given distance a between the antenna and the cutoff the optimization of active power transfer requires a plasma density $N_{\max} \cong N_{\text{CO}}\{1 + 1/(2\tanh^2(k_z M a))\}$ at a position close to the cutoff position. In this case the coupling depends as $k_z M / [\sinh(2k_z M a)]$ from the distance a and $|k_z M|$ if a is not too small and the power spectrum peak not too large around $|k_z M|$. The third point (iii) deals with the amount of wave reflection produced by the density gradient, which acts like a tapered line section in line transmission theory with a series of maxima and minima of reflection. To avoid too much reflection the density decay length l_{SOL} between N_{\max} and the high-density region has to be close to or exceed the first minimum of reflection occurring approximately for l_{SOL} equal to half the Alfvén wavelength ($\lambda_A = v_A/f$) of the high-density region. In the limit of large l_{SOL} the coupling value remains as large as the one obtained for a density $N = N_{\max}$ whatever the value of N_{bulk} . We have also shown the effect of departure with respect to the exponential decaying plasma profile. Coupling oscillations still remain for fatter or more hollow profiles. For sufficiently hollow edge profiles above N_{CO} the first coupling maxima are associated with strong resonances of the edge region (hollow profile + vacuum region) and they substantially exceed the asymptotic coupling value which is obtained for a homogeneous density $N = N_{\max}$ with its edge at the position of N_{CO} .

We have also given the closely related relations for the coupling to an inhomogeneous dielectric medium and a comparative summary of the coupling properties in view of dummy load or modelling applications is given in [7] and further discussed in the appendix.

Application to the considered reference edge profile for ITER has shown that this profile with its equivalent decay length of $l_{\text{SOL1}} = 2.5$ cm has the optimal edge density of each phasing case close to the corresponding cutoff and a not too large coupling reduction by reflection on the density gradient (l_{SOL1} is just below the first coupling maximum). However, the power capability can be increased by 20–46% if l_{SOL1} is brought to 4 cm (i.e. the local density gradient not exceeding $N(x)/l_{\text{SOL1}}$), the antenna–cutoff distance remaining that of the reference case for the considered phasing. The corresponding increase should be 40–55% if $l_{\text{SOL1}} = 6.5$ cm and the asymptotic improvement for very large l_{SOL1} and for the best edge density very close to the cutoff should reach 230–250%.

The effect of ‘low’ and ‘high’ profiles is considered as extreme pessimistic and optimistic edge profiles in front of the ITER antenna. The ‘low’ case has the same phasing hierarchy as the reference case but a coupling reduction of about 35% due to larger N_{CO} –antenna distance. The ‘high’ case, in contrast, leads to a huge coupling improvement up to 850% with a completely different hierarchy by bringing N_{\max} of phasing case 1 ($0\pi 0\pi$) close to N_{CO} at very short distance of the antenna.

The results also show that an increase in the bulk density with the same l_{SOL1} value has a (slight) beneficial effect: indeed the first coupling maximum occurs for lower values of l_{SOL1} but its amplitude is lower.

As already discussed in [5] the heating phasing 2 ($0 0 \pi \pi$) and co-current drive phasing ($0 \pi/2 \pi 3\pi/2$) have the best power capability for the profile ‘Sc2 short 17’, exceeding 20 MW per antenna for an antinode voltage of 45 kV in the eight feeding lines. This maximum voltage has to be reduced in some parts of the frequency domain in order to not exceed the limits of voltage, current or electric field in some sections of the antenna plug (see discussion in [17]). For the other considered profiles the best phasing cases are the same except for the profile ‘2010high’ where a plasma density close to N_{\max} of phasing case 1 ($0\pi 0\pi$) is brought near the antenna. This ‘most optimistic’ profile allows an extreme power capability for all phasing cases. With all considered profiles the power capability is higher than for the reference ‘Sc2 short 17’ with the exception of the extremely pessimistic one ‘2010low’ for which a maximum of 15 MW for $V_{\max} = 45$ kV is obtained.

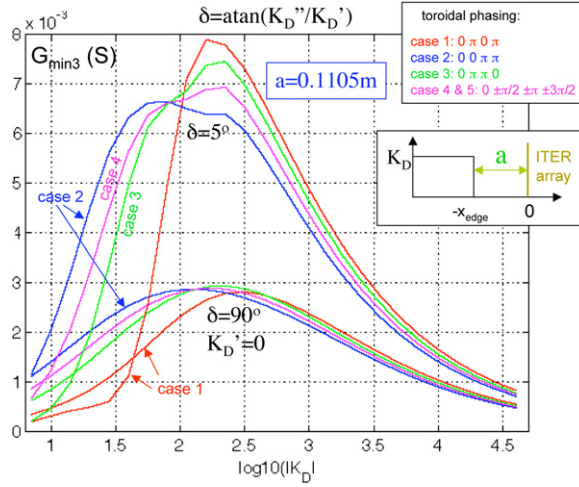


Figure A1. $G_{\min 3}$ of the different phasing cases as a function of $|K_D|$ for a single-step dielectric profile and for a loss angle $\delta = 5^\circ$ and 90° .

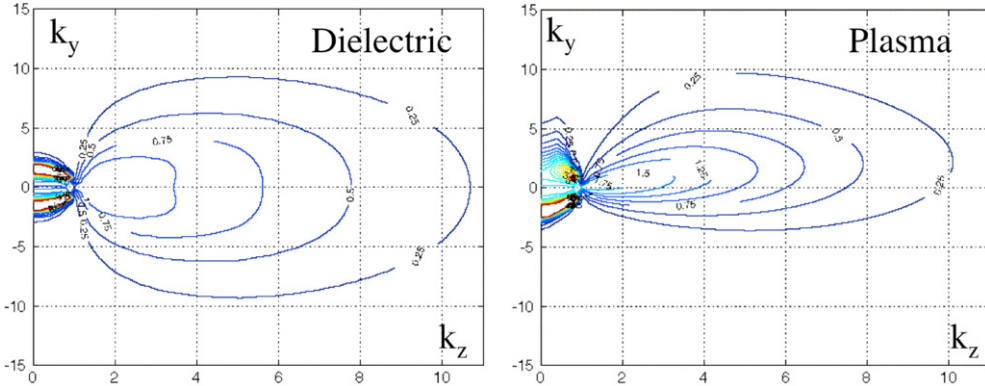


Figure A2. Comparison of the surface conductance k_z, k_y spectrum in front of the antenna for the plasma reference profile and its simulation by dielectric K_D profile.

There is also an influence of the plasma parameters (ion mix, magnetic field, frequency) on the coupling performance and this point is discussed in [18].

How to influence the density profile in a favourable way without affecting the confinement of ITER was not considered here but it is shown that the way to increase the coupling is to produce, e.g. by gas puff, a density a few times larger than the cutoff one as close as possible to the antenna and to avoid too steep a density gradient up to the bulk plasma.

Appendix. Further results and conclusions on the use of dielectric medium to simulate plasma loading

The comparative study of plasma and dielectric loading in view of its application for dummy load or modelling summarized in [7] has shown for an inhomogeneous dielectric load in front of the antenna array the same determining dependence of the position of the dielectric cutoff

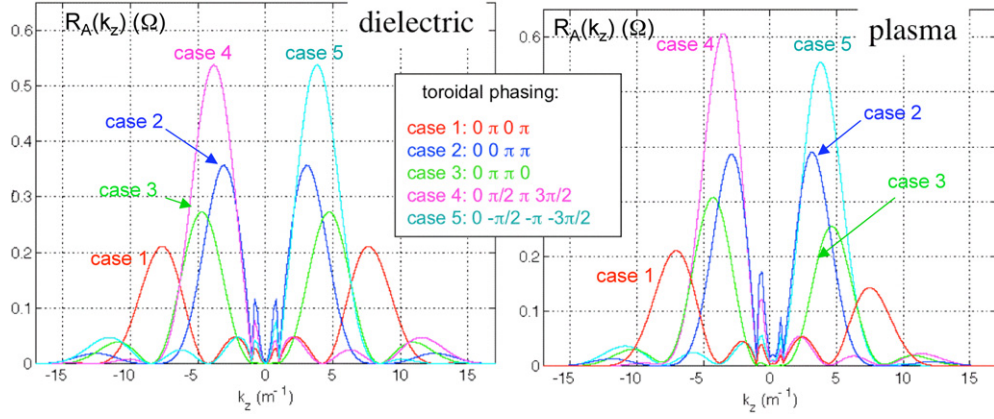


Figure A3. Comparison of the k_z antenna radiation resistance spectra (\propto to radiated power spectra) for the cases of figure A2.

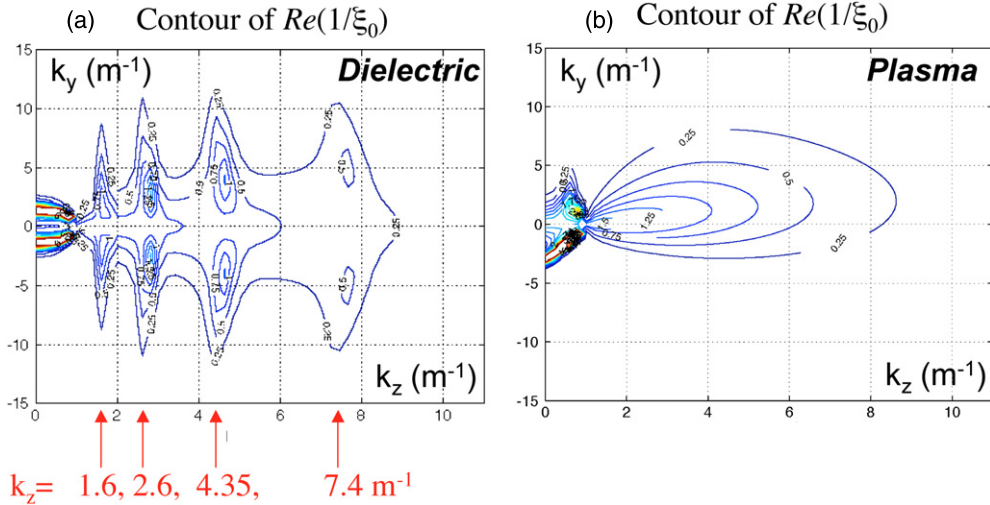


Figure A4. Surface conductance for a seven-step staircase approximate description of the reference density profile (see figure A5 bottom) (a) using a dielectric medium, (b) using steps of uniform plasma. The $|k_z|$ values of the surface waves excited along the four first steps in the dielectric case are indicated.

layer K_{DCO} (instead of N_{CO} for plasma) and the existence of an optimum dielectric constant value $K_D \text{ max}$ (instead of N_{max}) to be brought close to this cutoff to maximize the coupling. For a given value of $|K_D| = |K'_D + iK''_D|$ in the case of a lossy dielectric, the imaginary part of the dielectric constant decreases the optimal $|K_D|_{\text{max}}$ value but an optimal value remains for each phasing case even if $K'_D = 0$. This is shown in figure A1 where the mean minimum conductance $G_{\min 3}$ is plotted as a function of $|K_D|$ for a single-step dielectric constant profile in the case of low loss and in the limiting case of $K_D = iK''_D$.

The dielectric constant gradient between the cutoff and the bulk regions has also to be reduced below a threshold value expressed by the dielectric constant decay length $(l_{\text{SOL1}})_{\text{M1}} = \lambda_0 / \{2\sqrt{K_D}(x = x_{\text{bulk}})\}$ (for $k_y^2 \ll k_z^2$ and $k_0^2 \ll k_z^2$) corresponding to the first minimum of reflection to avoid a large decrease in reflection.

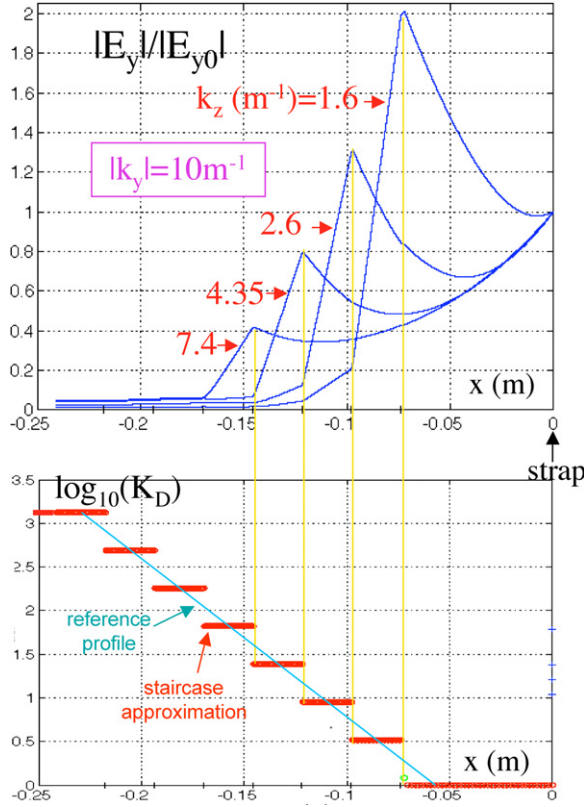


Figure A5. Bottom: seven staircases K_D approximation of the plasma reference profile. Top: evolution of $|E_y|/|E_{y0}|$ ($E_{y0} \equiv E_y(x = 0)$) of the Fourier wave components leading to surface wave along the jumps of the staircase steps.

The comparative study also shows that even in the absence of the description of the plasma anisotropy and particularly of its gyrotropy, the dielectric load can simulate fairly well the inhomogeneous plasma loading [7]. The best simulation of the considered ITER profiles (for frequency response and quantitative coupling measurements for the different toroidal phasing cases) is obtained by putting the plasma and low loss dielectric cutoff for all k_z at the same distance of the antenna [7]. This corresponds for $k_y^2 \ll k_z^2$ to the relation

$$K_{D,CO}(x) = \varepsilon_1(x) - \varepsilon_2(x) \quad \text{i.e. } K_D(x) = 1 + (\omega_{pi}(x))^2 / (\omega\omega_{ci} + \omega_{ci}^2) \quad (\text{a1})$$

for single species plasma.

Figure A2 compares the surface conductance $Re(1/\xi_0)$ for the plasma reference profile and its dielectric simulation according to equation (a1). The dielectric case is computed from the numerical integration in the non-uniform K_D profile assuming as for the plasma case no reflection in the bulk region, i.e. taking $\xi_{bulk} = (k_{\perp d}^2 - k_y^2)/k_{\perp d}^2$ with $k_{\perp d}^2 = k_0^2 K_{D,bulk} - k_z^2$. The asymmetry in $\pm|k_y|$ of the plasma conductance is due to its gyrotropy. Notwithstanding the lack of description of this effect, the power spectra $P(k_z)$ due to dielectric loading are very similar qualitatively and quantitatively to those of plasma loading as illustrated in figure A3 for all considered phasing cases. Only the asymmetry in $\pm|k_z|$ due to the gyrotropy and the steady poloidal magnetic field [5] is not simulated by the dielectric load.

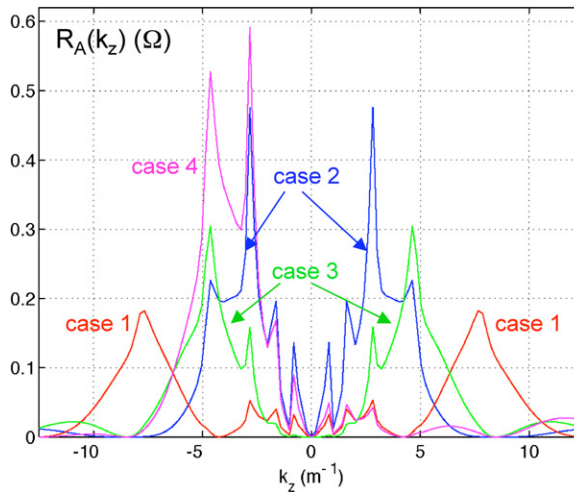


Figure A6. Deformed k_z antenna radiation resistance spectrum (\propto to radiated power spectrum) for the dielectric staircase of figure A5.

For numerical or technical reasons a multilayer profile is often preferred instead of the continuous dielectric profile. In this case the number of layers has to be chosen as large as possible to avoid strong resonances and surface wave effects on the power spectrum and coupling value. Indeed the dielectric multilayer load exhibits a surface conductance spectrum deformed by edge resonances like the one studied in section 8.2 for the extreme hollow plasma profile and by surface waves. This appears in the contour plot of the surface conductance given in figure A4(a) for the staircase dielectric constant profile shown at the bottom of figure A5. The seven stairs profile approximates the continuous $K_D(x)$ profile derived from (a1) to describe the reference plasma edge profile. One observe a series of maxima correlated with the excitation of surface waves when $|k_y|$ becomes large. This is shown in figure A5 where the electric field amplitude $|E_y|$ normalized with respect to its value at the front of the antenna ($|E_{y0}|$ at $x = 0$) is given as a function of x for the Fourier wave components of large $|k_y| = 10 \text{ m}^{-1}$ and for the $|k_z|$ values corresponding to the four first surface waves. They correspond to maximum field amplitude localized around the four first K_D jumps of the stairs. For lower values of $|k_y|$ a constructive interference with the reflection at the jump leads to maxima of coupling. Figure A6 shows the resulting strongly deformed radiated power spectrum for all phasing cases. The dielectric staircase approximation, unless for large number of stairs, leads to error in the coupling estimation (i) due to these resonances or modes propagating along the stairs and (ii) to the probable error in the cutoff location which now coincides with a dielectric constant jump. The surface waves are much less excited in the staircase approximation (for modelling purpose) of the plasma profile by stairs of homogeneous plasma as shown in the surface conductance spectrum shown in figure A4(b). This spectrum is for a seven stairs approximation of the reference plasma profile as for the dielectric case of figure A4(a).

Good simulation of the frequency response and power spectrum shape of the inhomogeneous plasma profile (as our reference case) can nevertheless be obtained with an homogeneous dielectric with $K'_D \cong 200$ in order to have K_D in the domain of $K_{D\max}$ corresponding to the different phasing cases and therefore remaining larger than all corresponding K_{DCO} [7]. Figure A7 gives the surface conductance spectrum of such a dummy

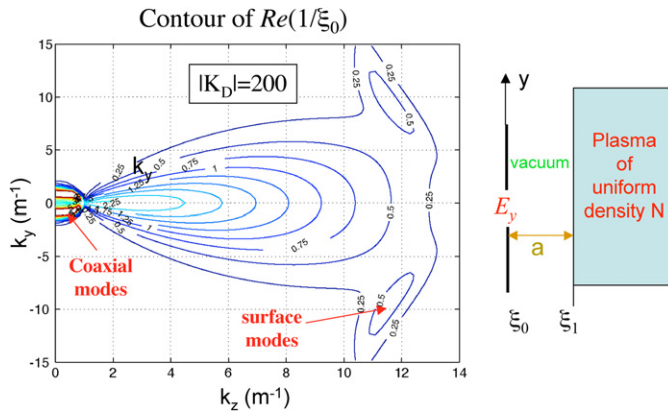


Figure A7. Surface conductance k_z, k_y spectrum for a dielectric dummy load with $|K_D| = 200$ and low loss angle $\delta = 5^\circ$.

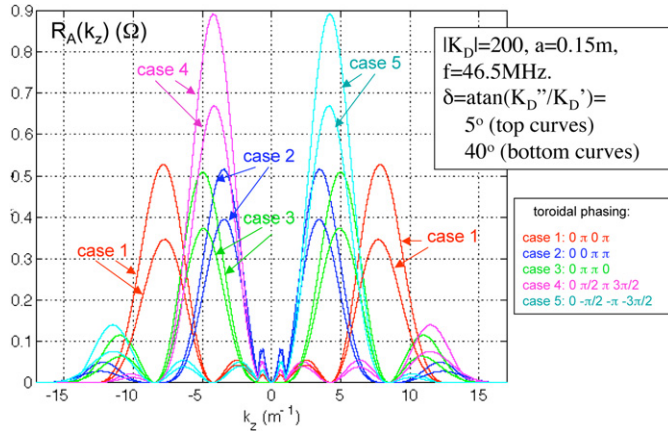


Figure A8. k_z antenna radiation resistance spectrum (\propto to radiated power spectrum) of a dielectric homogeneous dummy load of $|K_D| = 200$ at 46.5 MHz for the different phasing cases and for a loss angle $\delta = 5^\circ$ (top curves) and 40° (bottom curves).

load. One observes on this spectrum the presence of surface waves, which, for a single-step dielectric constant profile with low losses, have a dispersion relation:

$$|k_z| = k_0 \{(1 + K_D \tanh(|k_y|a)) / (1 + \tanh(|k_y|a))\}^{1/2} \quad \text{for } k_y^2 \gg k_z^2 \gg k_0^2. \quad (\text{a2})$$

They are practically not excited by the ITER array and the k_z power spectrum with the $K'_D \cong 200$ dummy load at mid-band is given for all phasing cases in figure A8. The spectra are not deformed and are qualitatively similar to the spectra shown in figure A3 for the ITER reference profile. The spectra are shown for two different values of the loss angle: the shape of the spectra remains the same when the loss angle increases but as previously stated the coupling decreases.

A water load is very effective for all phasing cases of ITER and behaves as the previous $K_D = 200$ load but its dielectric constant value $K_D = 81$ becomes smaller than the K_{DCO} value corresponding to phasing case 1 ($0\pi 0\pi$) in the lower part of the frequency band [7] and the response curve for this phasing is deformed.

A large loading domain covering the one expected for ITER (even in the presence of ELMs) can be scanned by varying the antenna–uniform dielectric load distance. For a given value of K'_D a small imaginary part of the dielectric constant K_D'' has to be chosen to avoid standing waves in the finite dielectric volume of the dummy load.

Euratom © 2011.

References

- [1] Messiaen A and Weynants R 1982 Heating in toroidal plasmas *Proc. 3rd Joint Varenna–Grenoble Int. Symp. (Grenoble, France, March 1982)* vol III EUR 7979 EN (Brussels: Commission of European Communities) p 1107
- [2] Bilato R *et al* 2005 *Nucl. Fusion* **45** L5
- [3] Weynants R 2009 *Proc. 18th Topical Conf. on Radiofrequency Power in Plasmas* (Melville, NY: APS) *AIP Conf. Proc.* **1187** 3
- [4] Nightingale M *et al* 2009 *Proc. 18th Topical Conf. on Radiofrequency Power in Plasmas* (Melville, NY: APS) *AIP Conf. Proc.* **1187** 213
- [5] Messiaen A *et al* 2010 *Nucl. Fusion* **50** 025026
- [6] Milanesio D and Maggiora R 2010 *Nucl. Fusion* **50** 025007
- [7] Messiaen A *et al* 2011 *Fusion Eng. Des.* doi:10.1016/j.fusengdes.2011.01.035
- [8] Lamalle P *et al* 2009 *Proc. 18th Topical Conf. on Radiofrequency Power in Plasmas* (Melville, NY: APS) *AIP Conf. Proc.* **1187** 265
- [9] Messiaen A *et al* 2009 *Nucl. Fusion* **49** 055004
- [10] Loarte A 2008 private communication
- [11] Loarte A *et al* 2008 *Proc. 22nd Int. Conf. on Fusion Energy 2008* (Geneva, Switzerland, 2008) CD ROM file IT/P6-13
- [12] Dumortier P *et al* 2009 *Fusion Eng. Des.* **84** 707
- [13] Messiaen A *et al* 1984 Heating in toroidal plasmas *Proc. 4th Joint Varenna–Grenoble Int. Symp. (Rome, Italy, March 1984)* vol I, ed H Knoepfel and E Sindoni, p 315
- [14] Messiaen A *et al* 1986 *Proc. 13th European Conf. on Fusion and Plasma Heating* (Schliersee, Germany, April 1986) vol 10C (ECA) p 125
- [15] Collins R 2001 *Foundations for Microwave Engineering* 2nd edn (*IEEE Press Series on Electromagnetic Wave Theory*) (Hoboken, NJ: Wiley)
- [16] Carpentier S and Pitts R 2010 *Report ITER_D_33Y59M*
- [17] Dumortier P *et al* 2011 Invited paper, *Proc. 19th Topical Conf. on Radiofrequency Power in Plasmas* (Newport, RI) (*AIP Conf. Proc.* at press)
- [18] Messiaen A *et al* 2011 *Proc. 19th Topical Conf. on Radiofrequency Power in Plasmas* (Newport, RI) (*AIP Conf. Proc.* at press)